

This pdf file contains all figure pages in the dissertation:

SEDIMENTOLOGY, PETROGRAPHY, AND TECTONIC SIGNIFICANCE
OF CRETACEOUS TO LOWER TERTIARY
DEPOSITS IN THE TINGRI-GYANGTSE AREA, SOUTHERN TIBET

By

Bin Zhu

A Dissertation

Submitted to the University at Albany, State University of New York

in Partial Fulfillment of

the Requirements for the Degree of

Doctor of Philosophy

College of Arts & Sciences

Department of Earth & Atmospheric Sciences

2003

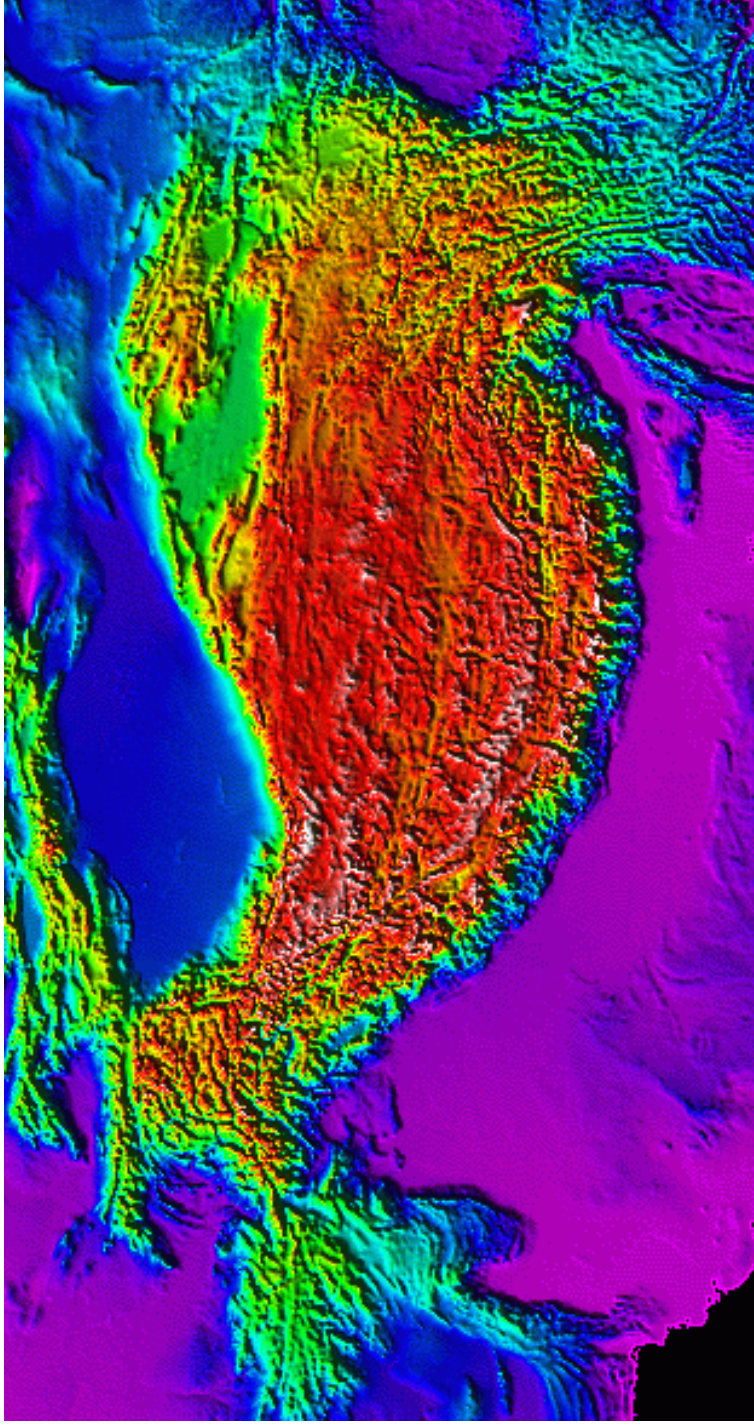


Figure 1.1 Himalayas-Tibetan Plateau Topography (from <http://www.geo.cornell.edu>). This image is a false-color, shaded relief image with illumination from the northwest. The shadowing gives an indication of local relief while color indicates elevation as follows: magenta=sea-level; blue=1000m; cyan=2000m; green=3000m; yellow=4000m; red=5000m; white=6000m and above.

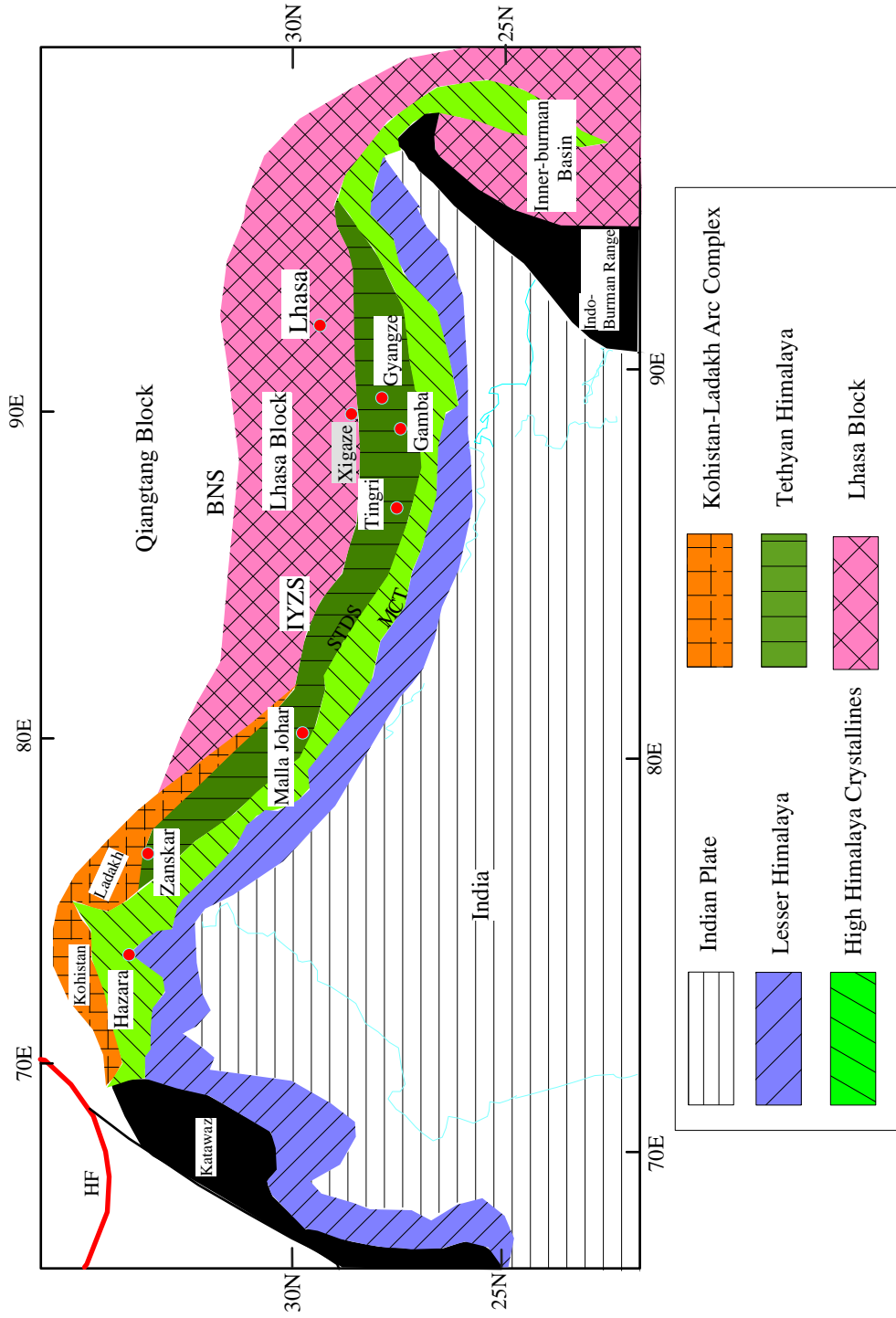


Figure 1.2 Regional geological map of Tethyan Himalaya (modified after Rowley, 1996)
 BNS: Banggong-Nujiang Suture IYZS: Indus-Yarlung-Zangbo-Suture, MCT: Main-Central-Thrust,
 STDS: Southern-Tibet-Detachment-System

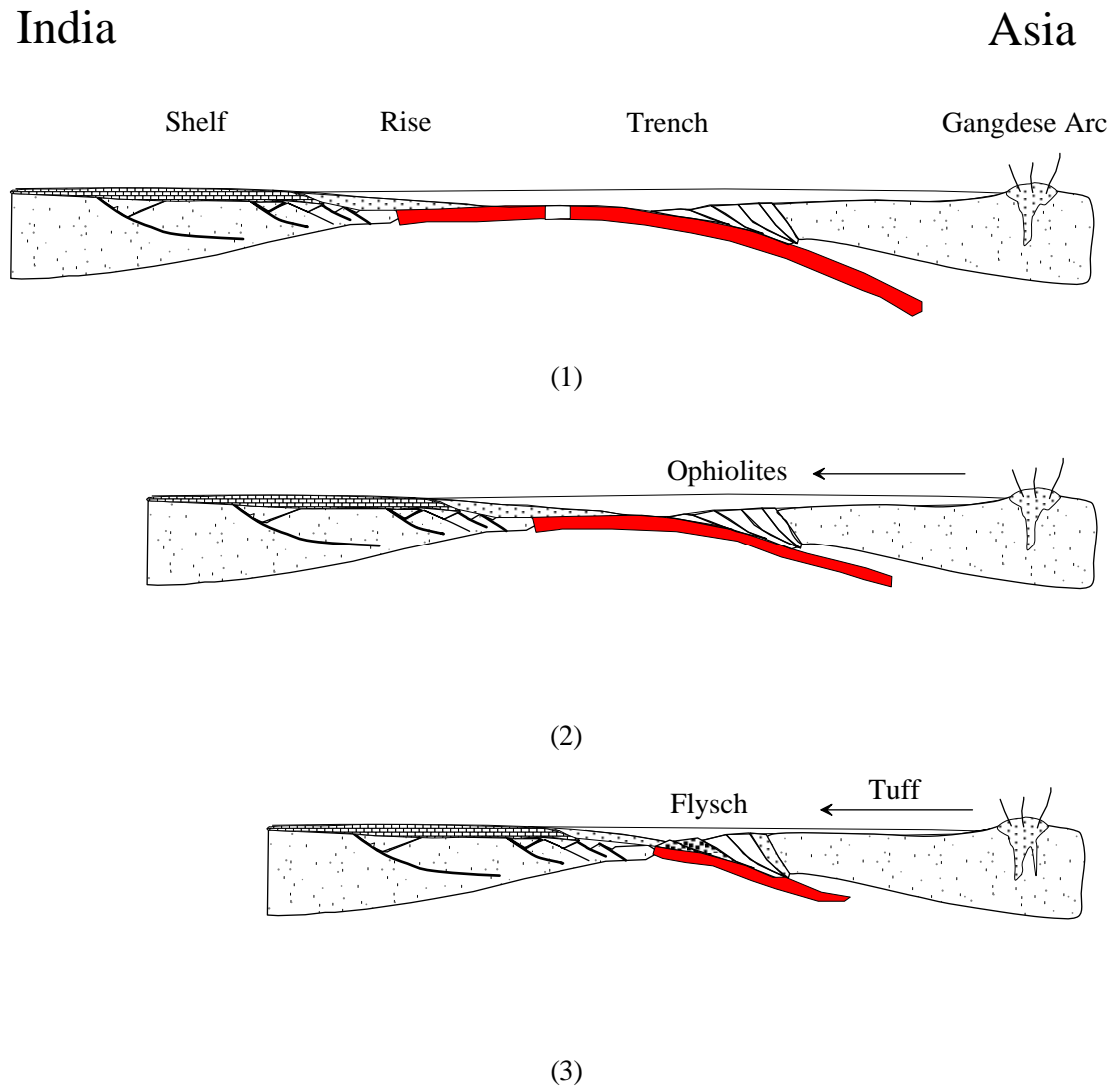


Figure 1.3 Schematic cross-sections of the India-Asia convergence up to the initiation of collision (modified after Rowley and Kidd, 1981). (1) Cretaceous; (2) Paleocene; (3) Eocene.

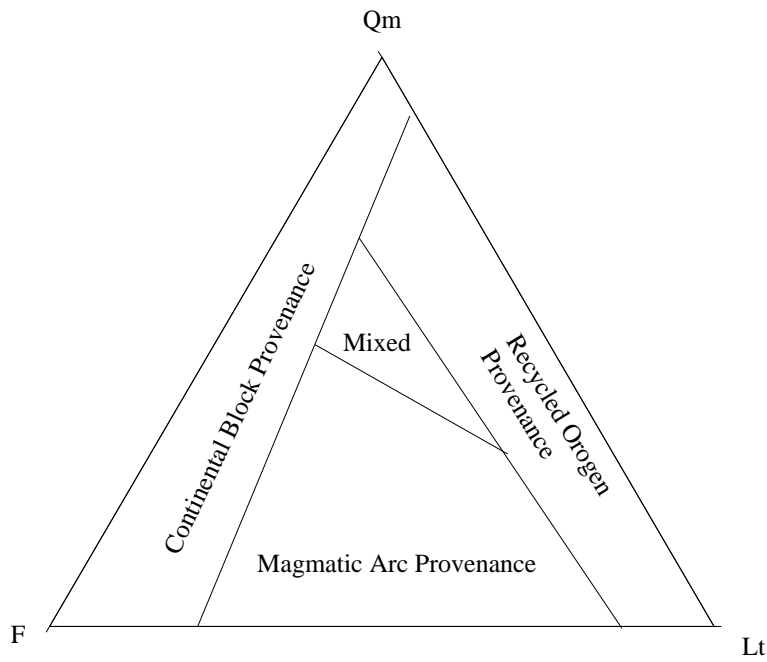
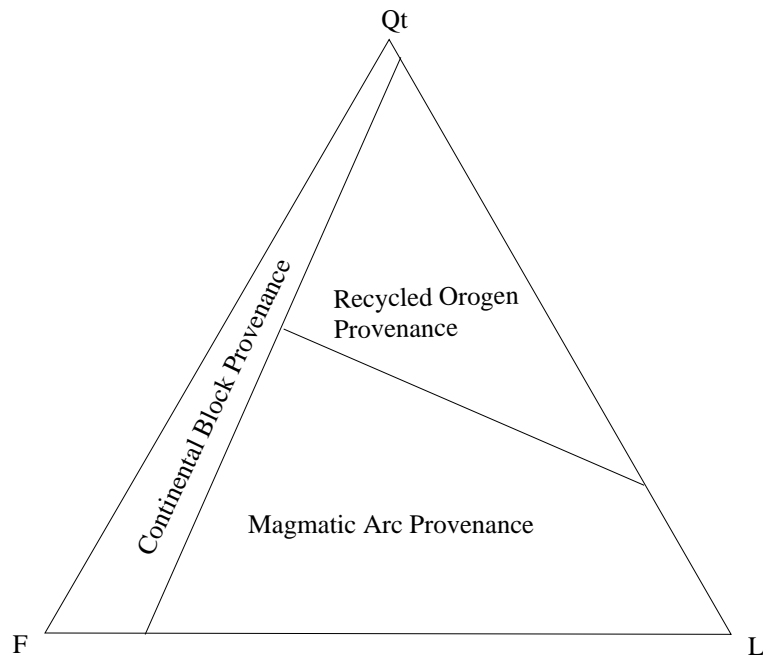


Figure 1.4 Detrital mode distribution in three major tectonic settings. After Dickinson et al. (1983).

Qt: monocrystalline quartz+polycrystalline quartz; Qm: monocrystalline quartz; F: feldspar, L: rock fragments; Lt: rock fragments+polycrystalline quartz.

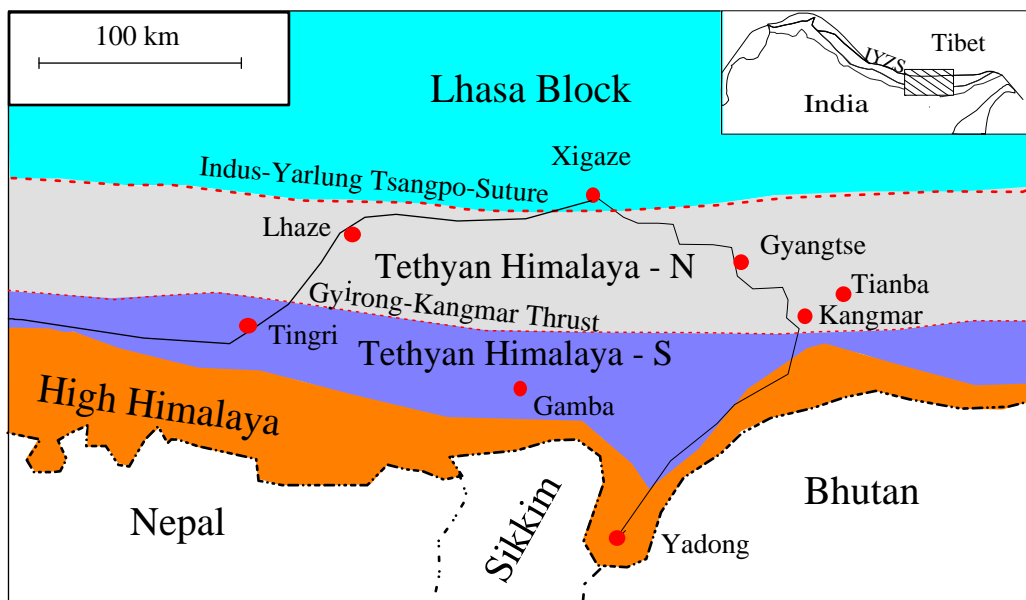


Figure 2.1 Simplified geologic map of Tingri-Gyangtse area, southern Tibet (modified after Willems et al., 1996). The inset map shows this region located in the Himalaya system.

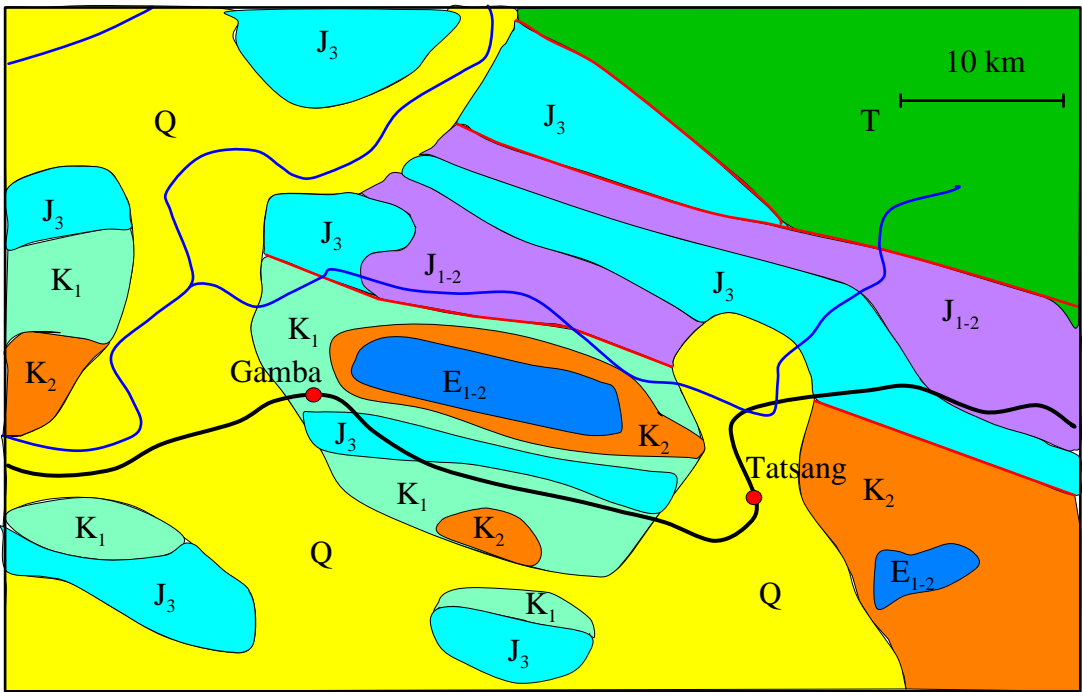


Figure 2.2 Simplified geologic map of the Gamba region (modified after geologic map (1:1,500,000) in Xizang BGMR, 1992).

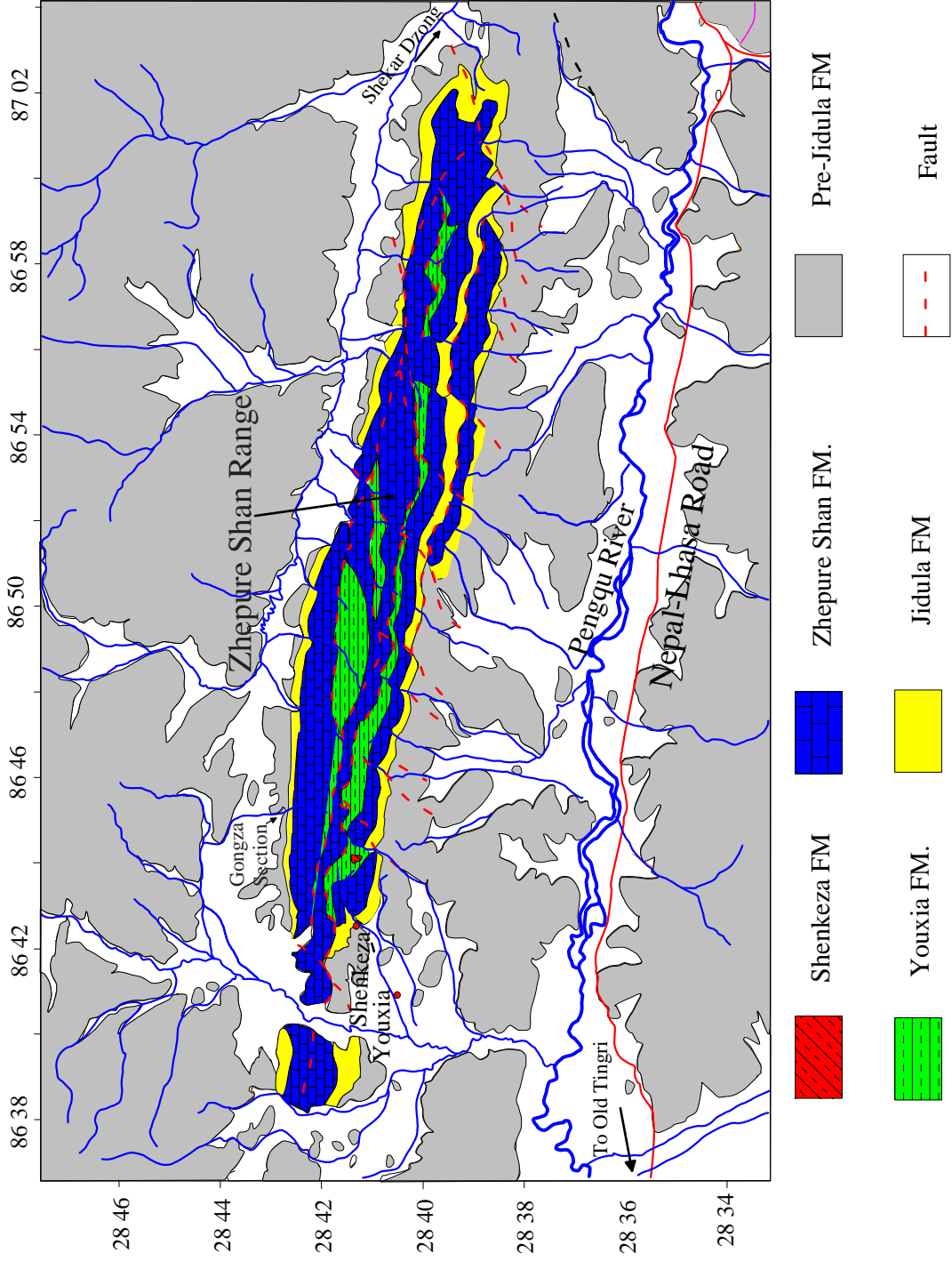


Figure 2.3 Geologic map of the Zhepure Shan Mountain (based on field observations and image interpretation (Kidd)). Geographic coordinates in degrees, minutes.

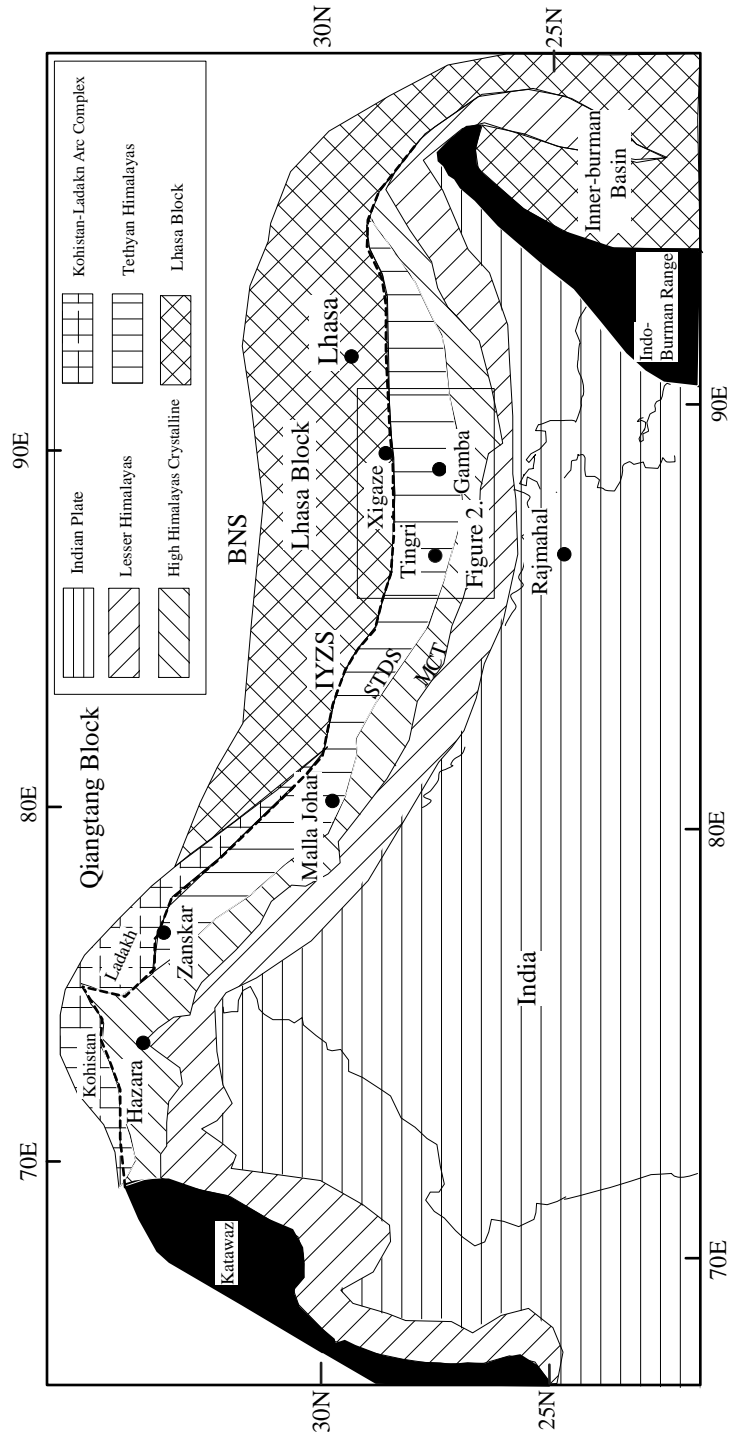


Figure 3.1 Regional geological map of Tethyan Himalaya (after Rowley, 1996). BNS: Banggong-Nujiang Suture IYZS: Indus-Yarlung-Zangbo-Suture, MCT: Main-Central-Thrust, STDS: Southern-Tibet-Detachment-System.

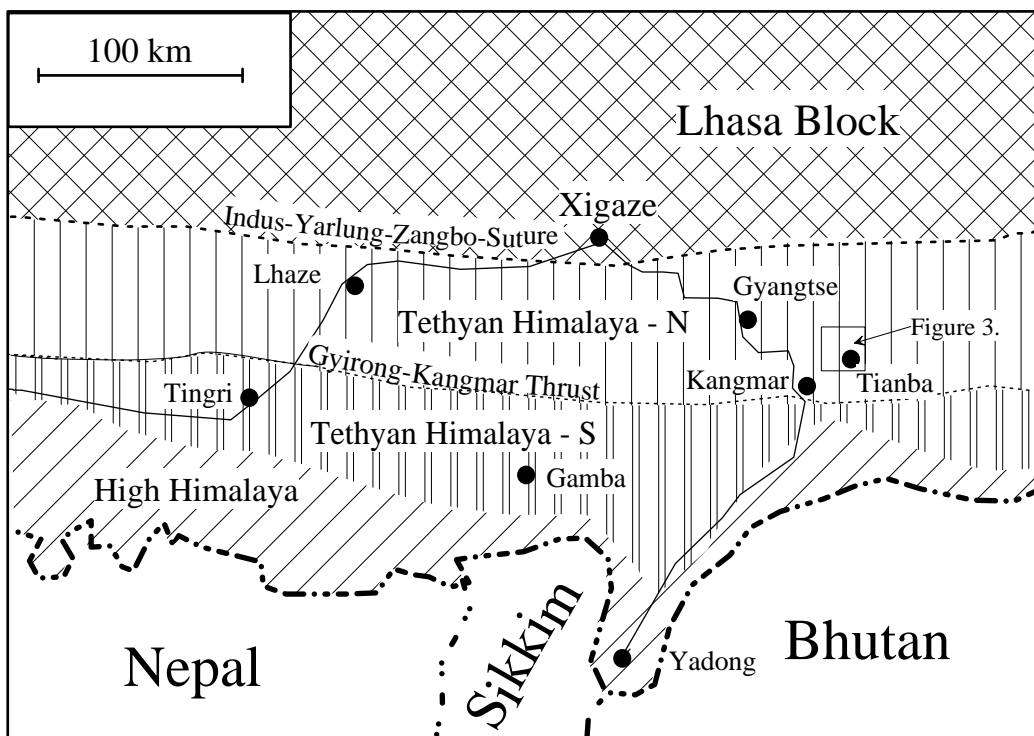
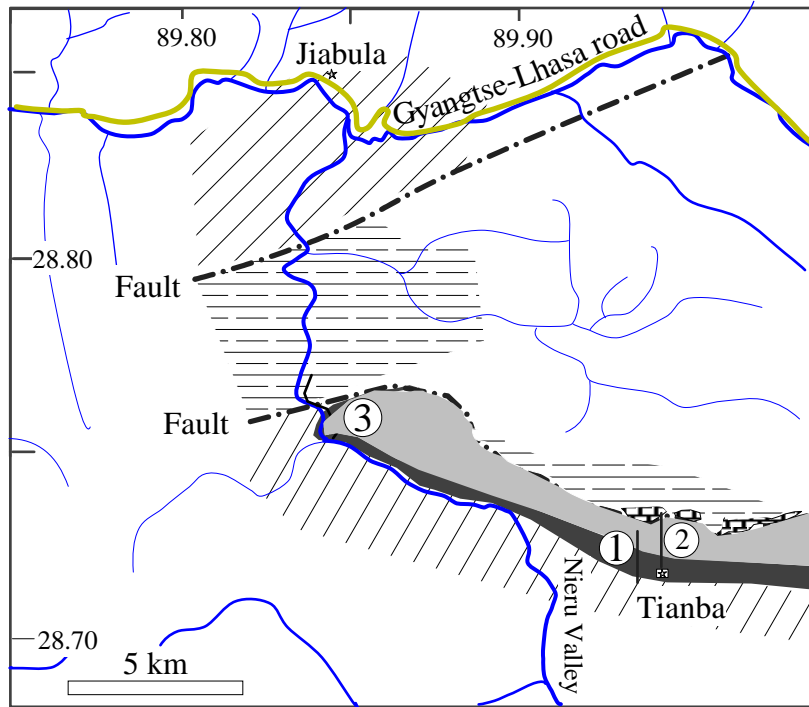




Figure 3.2 Simplified tectonic map of the study area (after Willems et al, 1996)



 Melange (area of pink limestone blocks shown)

 Tianba Flysch and overlying shales

 Black cherts and shales

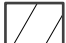
 Grey shales, quartzites and marls

Figure 3.3 Sketch geologic map at Tianba showing three measured sections 1-3. Note: Rivers are traced from the 1:100,000 topographic map

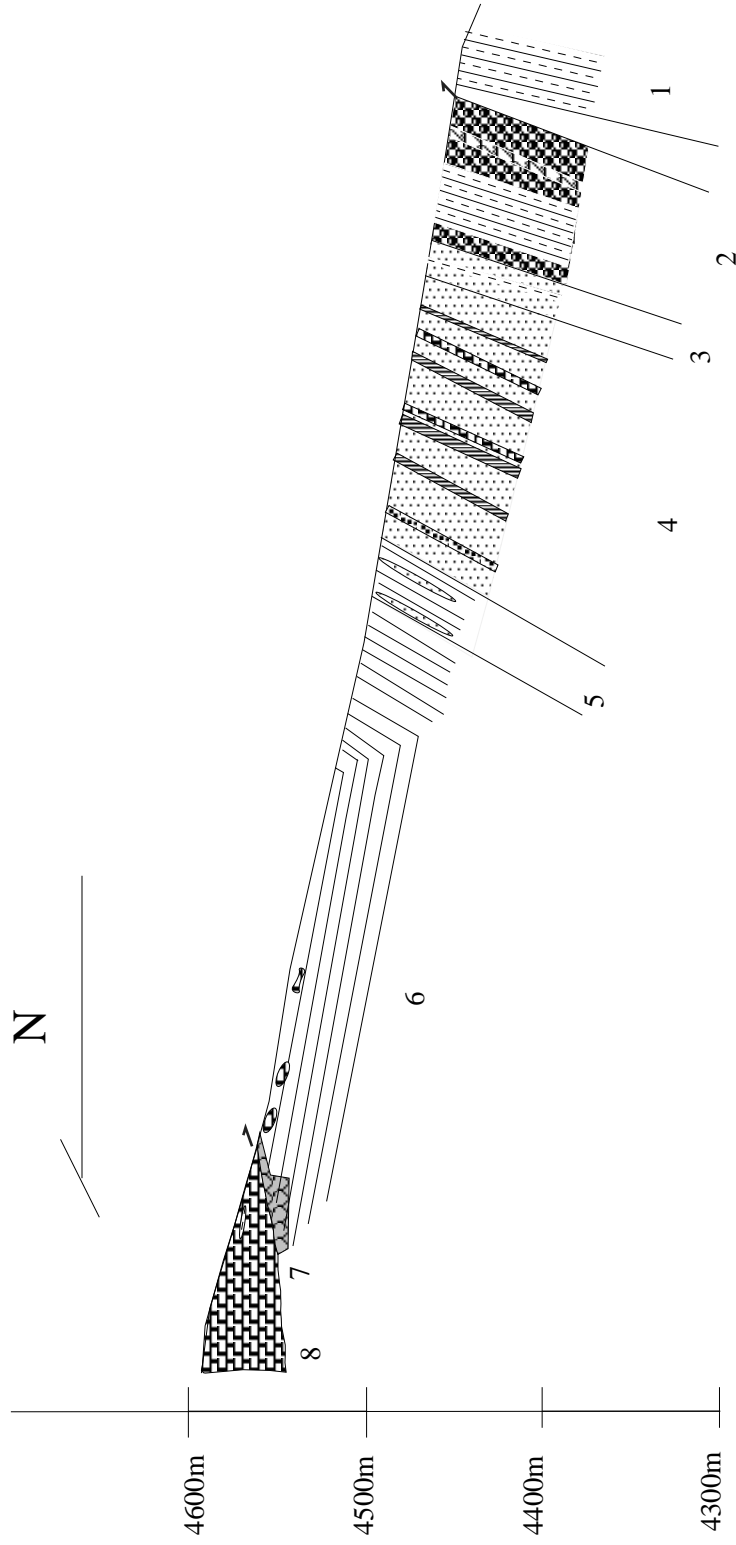


Figure 3.4. Tianba cross-section (section 2, see figure 3.3 for location) Horizontal scale=vertical scale
See Figure 3.11 for explanation of lithologic units and ornaments.



Figure 3.5 View to north of Tianba section. Dark grey shales and cherts are of early Cretaceous sediments in the river valley and the lower slopes of the hills beyond; tan-orange band is the Tianba Flysch; pink-purple rocks above this are fault-juxtaposed late Cretaceous limestones and shales. [The author, Bin Zhu, in this picture]



(1)



(2)

Figure 3.6 Sedimentary structures in the Tianba Flysch
(1) Ripple marks; (2) Sole marks.



Figure 3.7 Well-bedded turbidite sandstones with shale interbeds in the center part of the Tianba Flysch. View to east, section youngs to north (left).



Figure 3.8 Top of the Tianba Flysch, north of Tianba village. The uppermost thick-bedded sandstone of the Tianba Flysch is on the right. View to ENE, section youngs to north (left). The dark grey shales conformably overlie the Tianba flysch.



Figure 3.9 Sideritic sandstone bed showing graded-bedding. Abundant Cr-rich spinels are found in these sandstones.



Figure 3.10 Outsized (up to 1 m across) calcareous nodules in the greenish-grey shales, north of Tianba village. View to NE. One small nodule (10 cm across) yielded an ammonite. [Dr. B. Zhang in this picture]

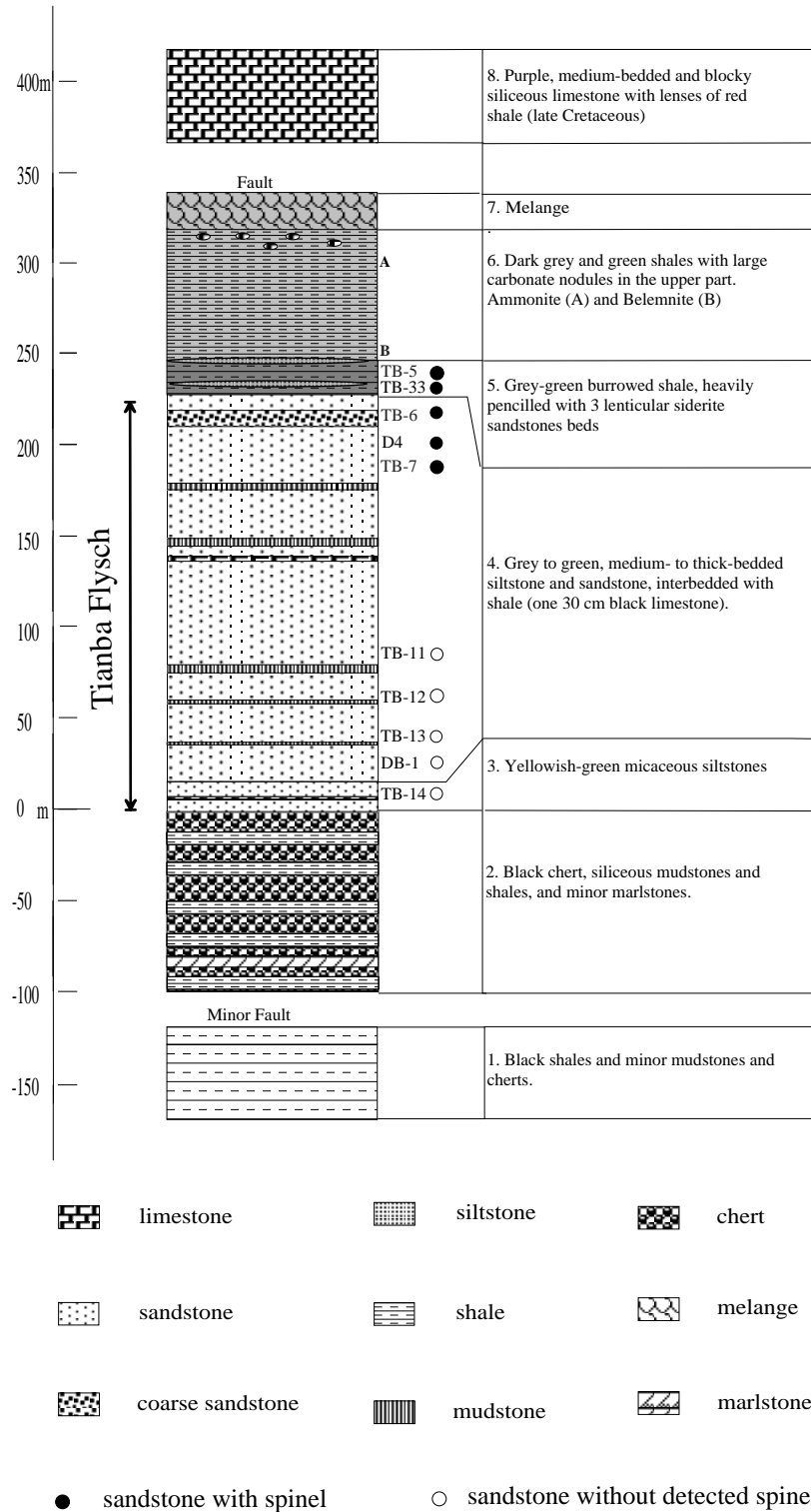


Figure 3.11 Measured Section (2), north of Tianba village. See Figure 3.3 for location.

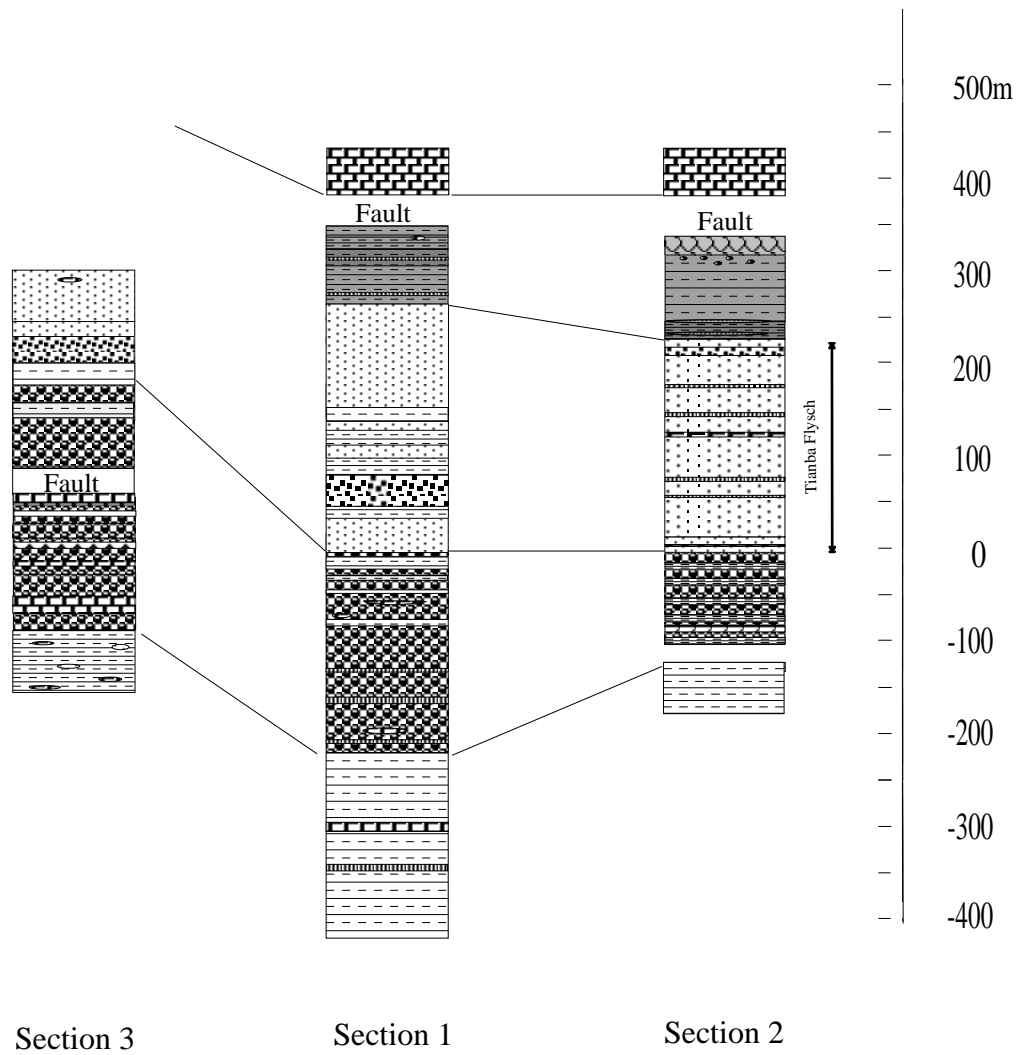


Figure 3.12 Measured stratigraphic sections at Tianba. Section locations are shown in Figure 3.3 See Figure 3.11 for explanation of the lithologic ornaments.

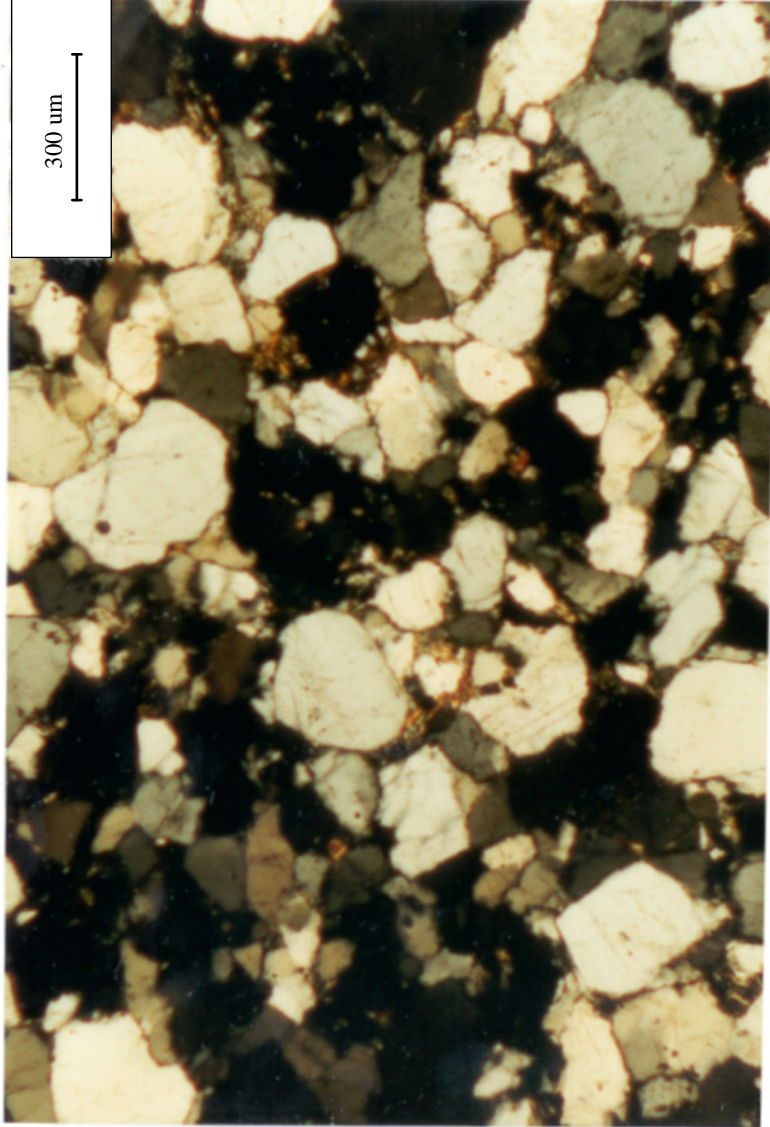


Figure 3.13 Photomicrograph (crossed polars) of quartz-rich sandstone in the basal part of western section (section 3 in Figure 3.3). Quartz grains are mostly monocrystalline, and the rock is well-sorted.

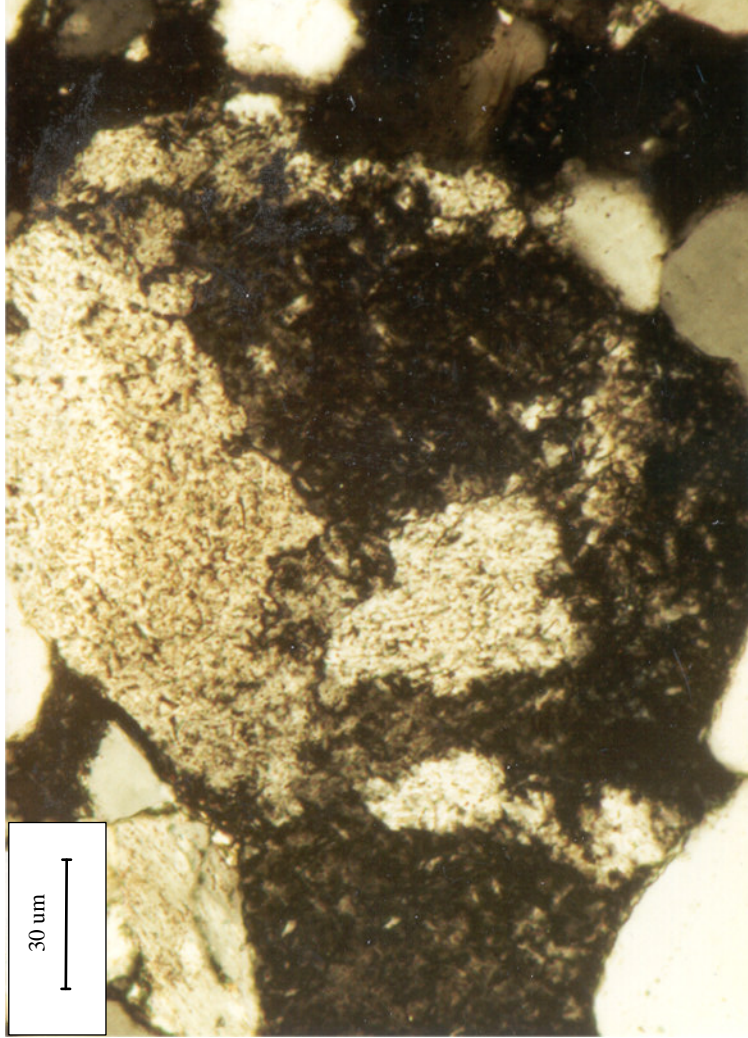
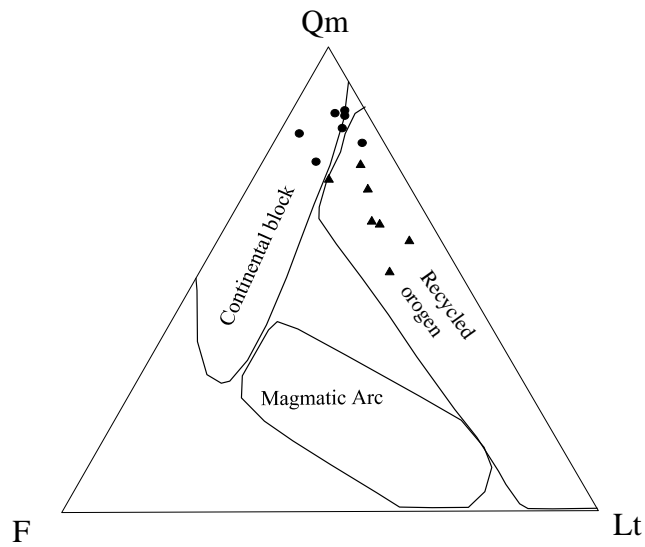
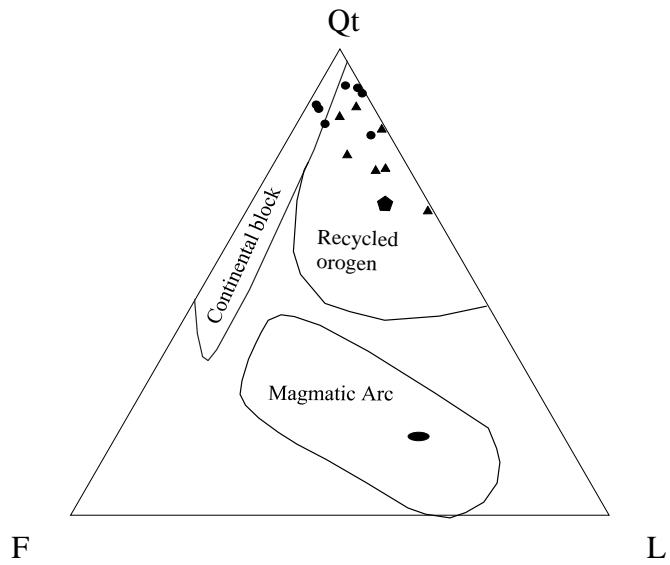


Figure 3.14 Photomicrograph (crossed polars) of a metamorphic rock fragment in the quartz-rich sandstones in the basal part of western section (section 3, see figure 3.3 for location).



- | | | | |
|---|-----------------|---|--|
| ▲ | Greywackes | ● | Chulung La Arenite
(Garzanti, et al., 1987) |
| ● | Quartz arenites | ◆ | Giumal sandstone
(Garzanti, et al., 1987) |

Figure 3.15 Detrital mode plot of sandstones in the Tianba sections. Tectonic fields from Dickinson and Suczek, 1979. Giumal sandstones and Chulung La Arenite from Zanskar are shown for reference on the QtFL plot.

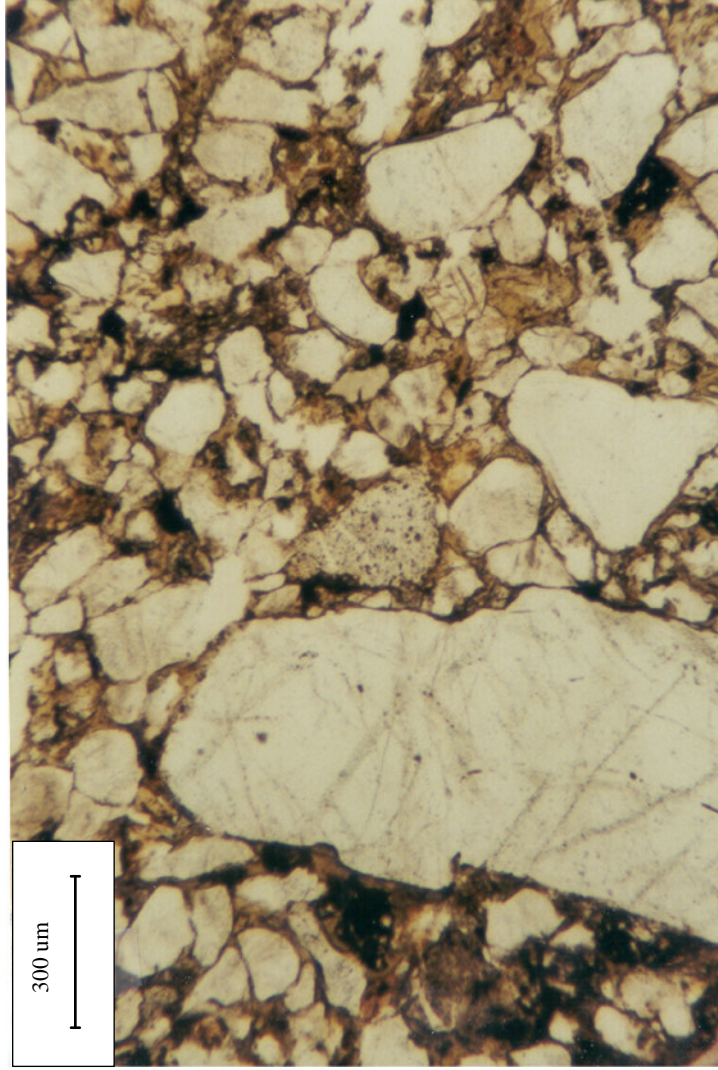


Figure 3.16 Photomicrograph (plane polars) of greywackes in the Tianba measured section. Note angular quartz grains are poorly-sorted, and there are some feldspar grains (dusty/dirty looking compared with clearer quartz grains).

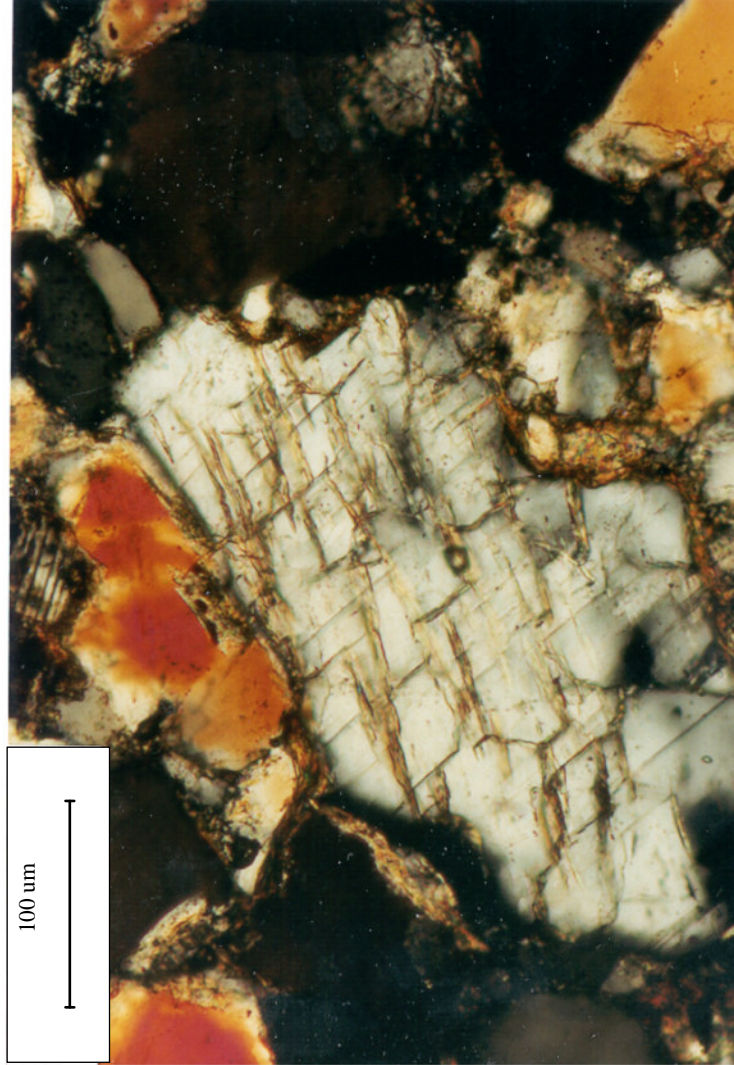


Figure 3.17 Photomicrograph (crossed polars) of feldspar (perthite) in the greywackes of the Tianba section 2 (see figure 3.3 for location).



Figure 3. 18 Photomicrograph of a volcanic rock fragment composed of plagioclase phenocrysts within fine-grained ground mass. This indicates that there was a significant volcanic source for the Tianba Flysch.

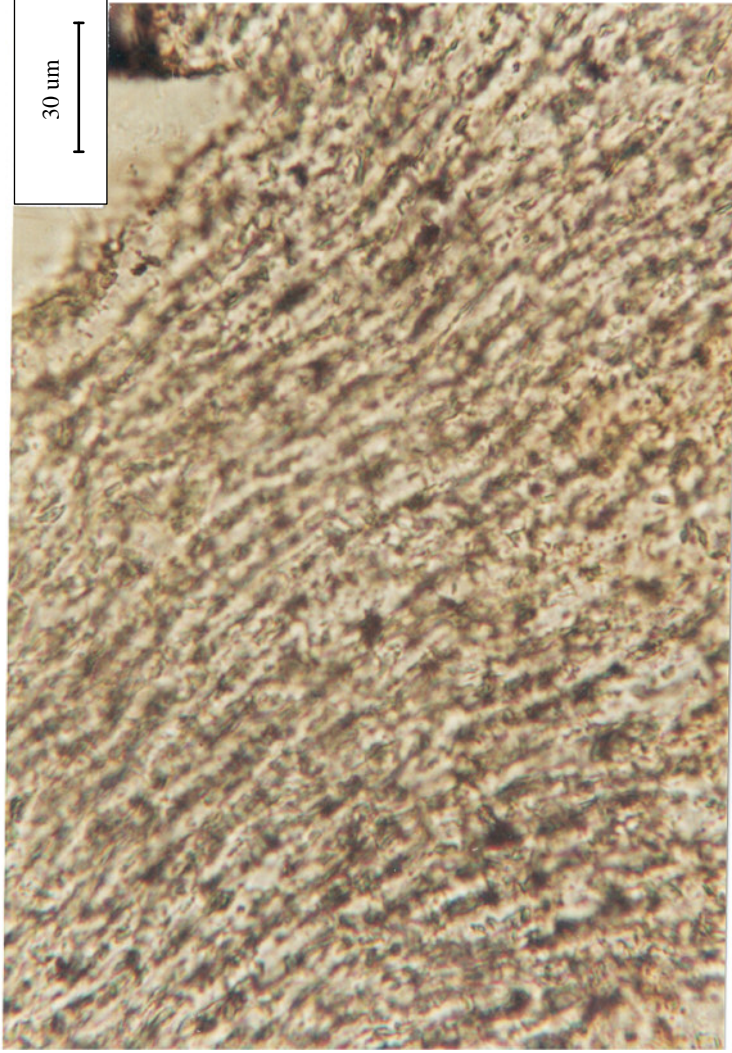


Figure 3.19 Photomicrograph (crossed polars) of a rock fragment with trachytic texture in TB6 sample in the Tianba section 2 (see figure 3.3 for section location).

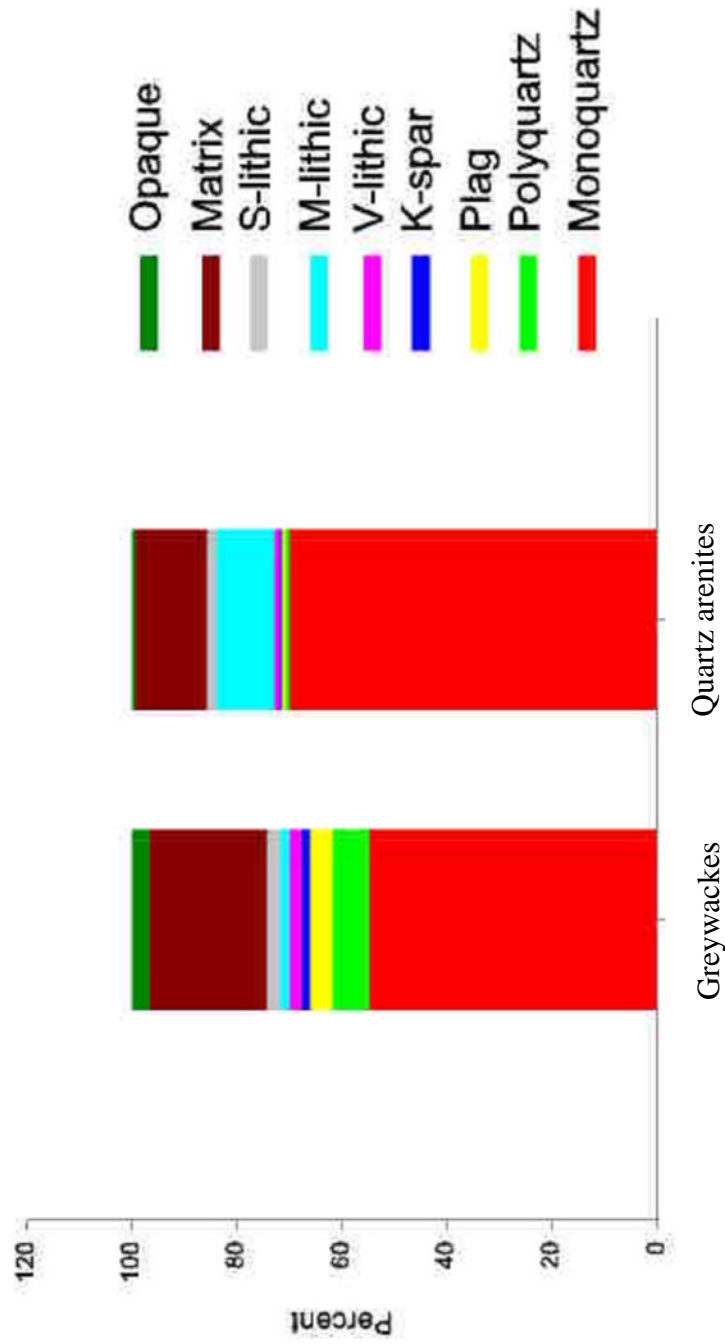
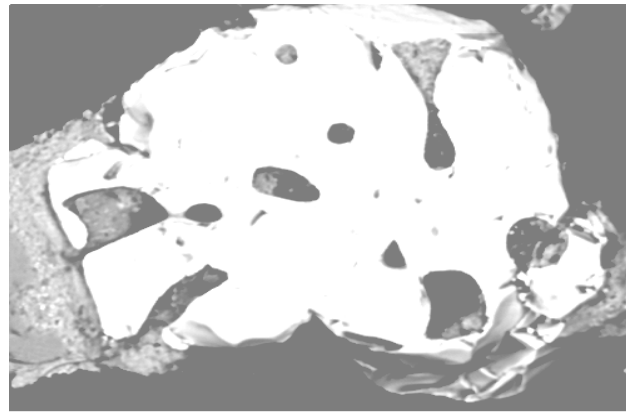


Figure 3.20 Histogram showing the different detrital modes between quartzite and greywackes in the Tianba sections. These sandstones have similar quartz contents, while there are more matrix, feldspar, volcanic lithics and less metamorphic lithics in the greywackes compared to the quartzites.

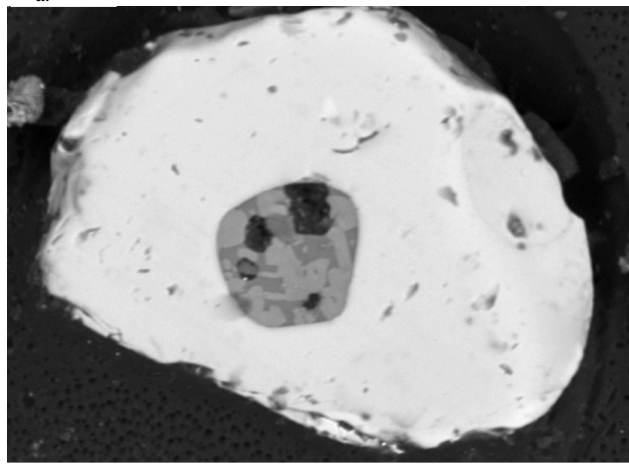
Monoquartz: monocrystalline quartz; Polyquartz: polycrystalline quartz; Plag: plagioclase; K-spar: K-feldspar; V-lithic: volcanic lithics; M-lithic: metamorphic lithics; S-lithic: sedimentary lithics; opaque: opaque minerals.



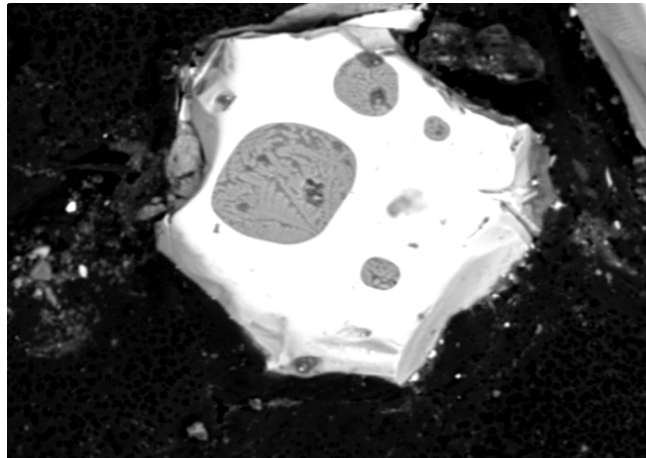
Figure 3.2.1 Chemical compositions of detrital Cr-rich spinels using pairs plot from S-plus



a.



b.



c.

Figure 3.22 Backscattered electron images of melt inclusions in the detrital spinels from Tianba Flysch.

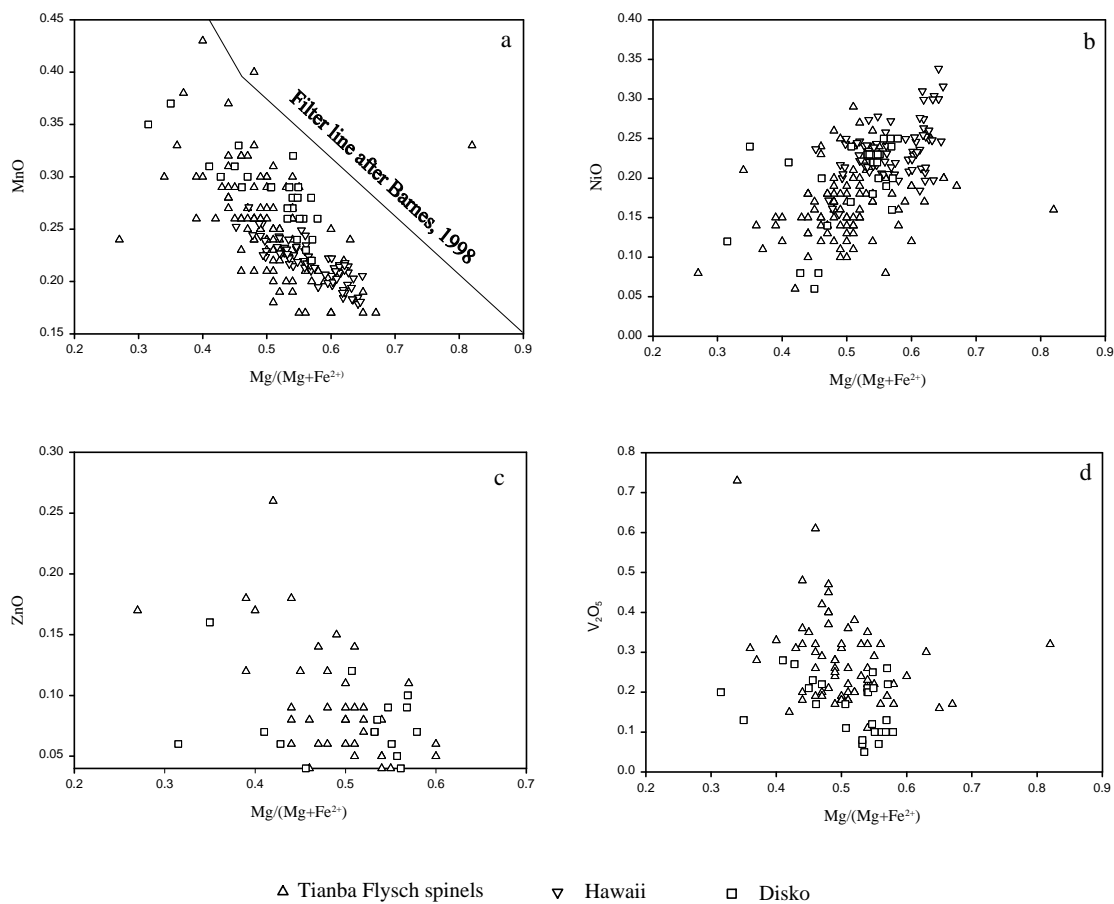
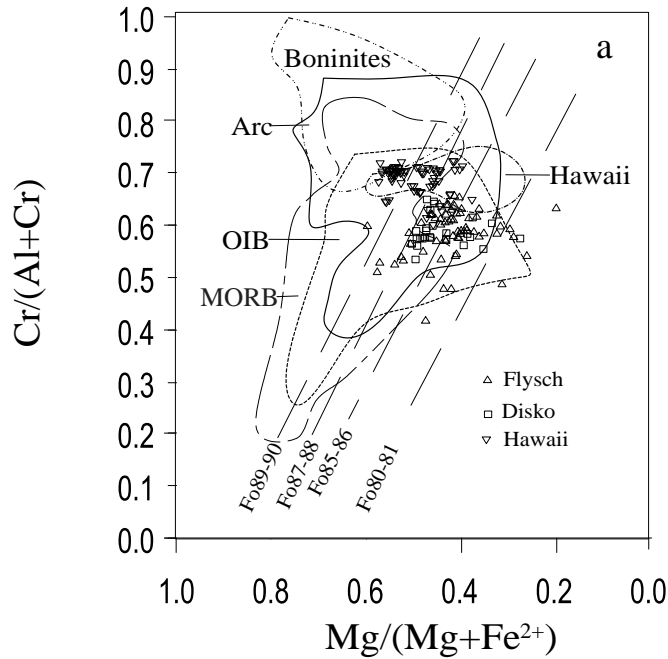


Figure 3.23 Covariation of minor elements with $Mg/(Mg+Fe^{2+})$ in spinel
 (For comparison, data from Hawaii and Disko are also shown):
 a. MnO vs. Mg#; b. NiO vs. Mg#; c. ZnO vs. Mg#; d. V_2O_5 vs. Mg#.



Isopleths of olivine Fo (dashed lines) from Kamenetsky et al, 2001

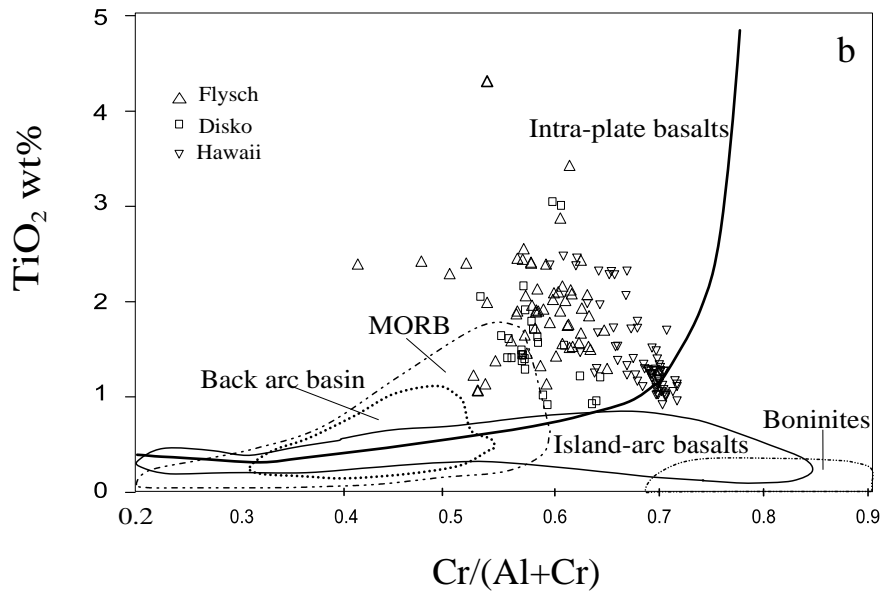


Figure 3.24 Major element contents of spinels and tectonic setting discriminant plot:
 a. Cr/(Cr+Al) vs. Mg/(Mg+Fe²⁺) after Barnes and Roeder, 2001;
 b. TiO₂ vs. Cr/(Cr+Al) after Arai, 1992.

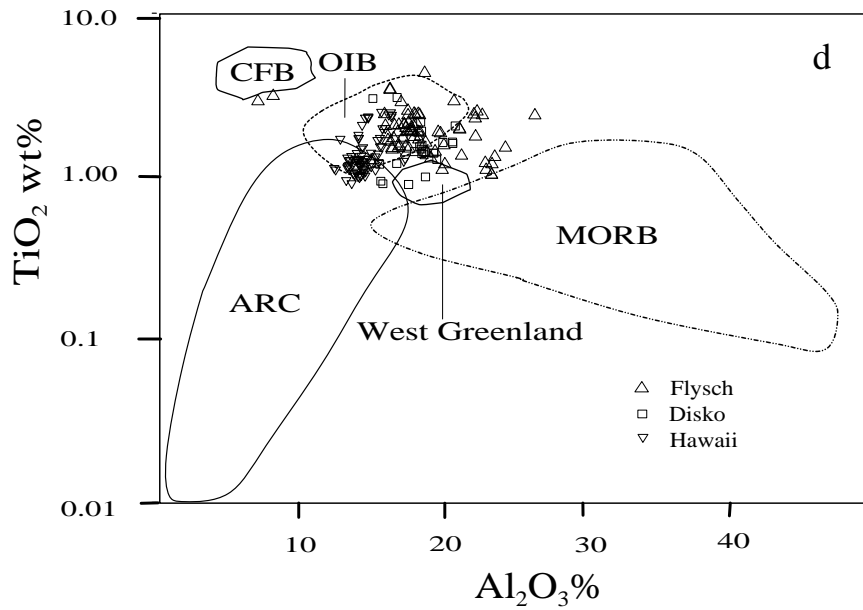
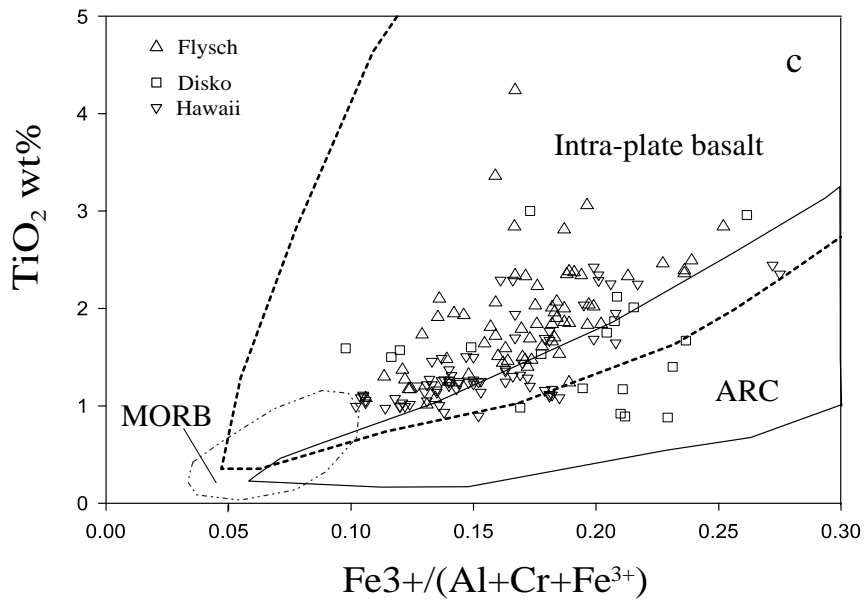


Figure 3.24(continued) Major element contents of spinels and tectonic setting discriminant plot:
 c. TiO_2 vs. $\text{Fe}^{3+}/(\text{Al}+\text{Cr}+\text{Fe}^{3+})$ after Arai, 1992;
 d. TiO_2 vs. $\text{Al}_2\text{O}_3\%$ after Kamenetsky et al, 2001.

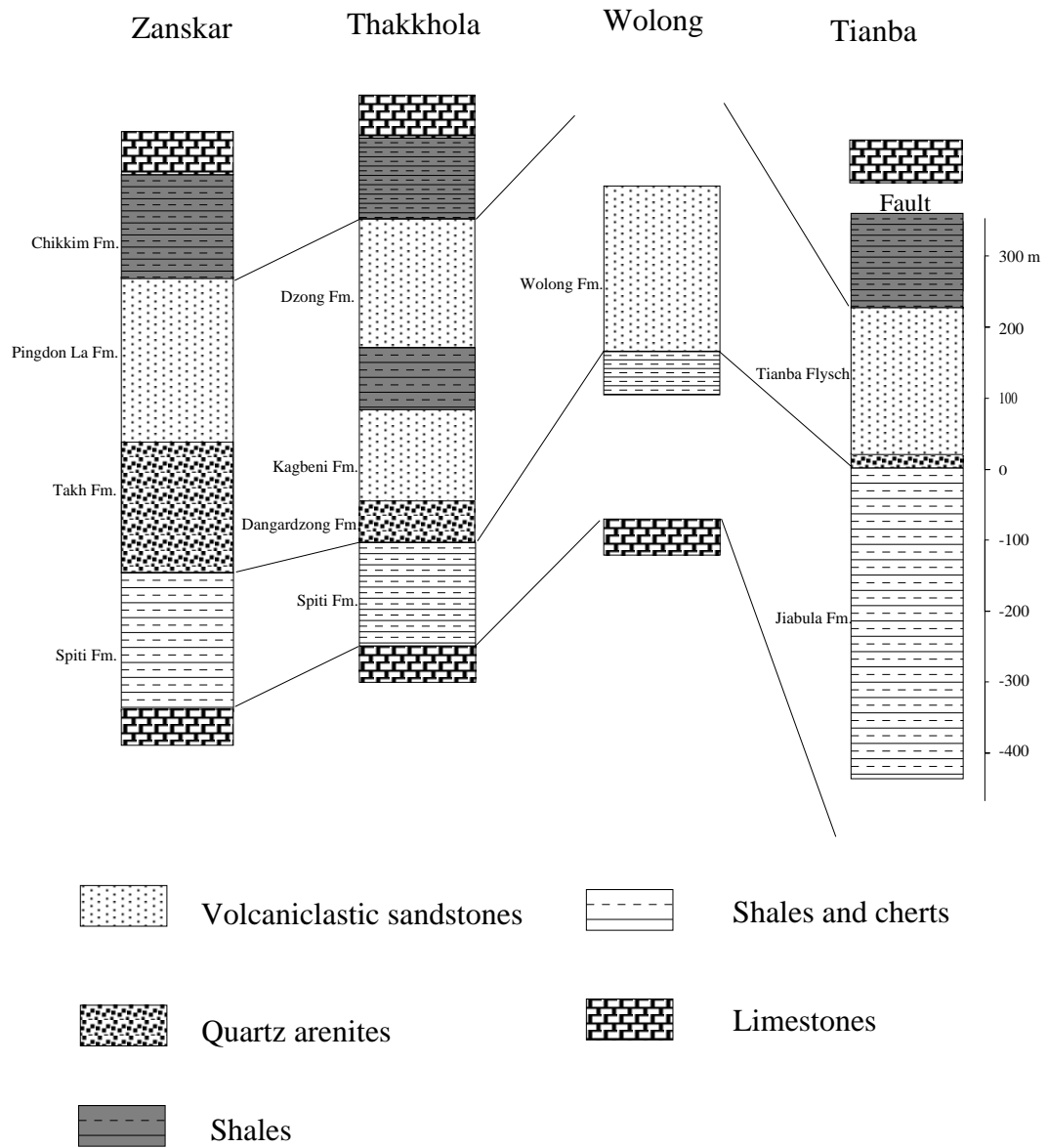
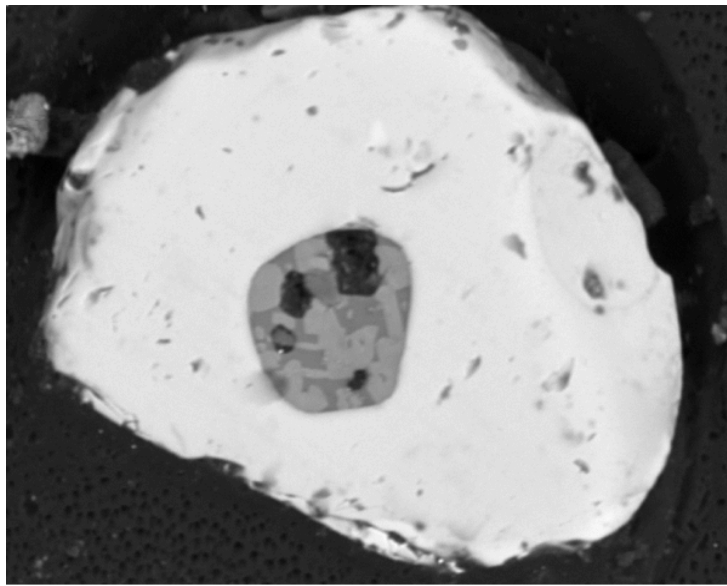
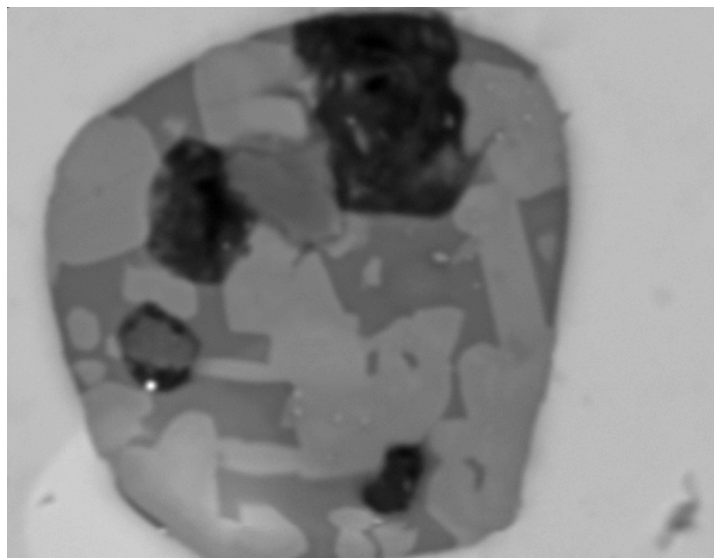


Figure 3.25 Comparison of lithostratigraphy between Tianba, Zanskar (after Garzanti, 1993), Thakkhola (Garzanti, 1999) and Wolong (Jadoul, et al. 1998).



BE 3-2-7 30 μ m

(a)



BE 3-2-7-detail 10 μ m

(b)

Figure 4.1 (a) Backscattered electron images of a crystallized melt inclusion (grey) in Cr spinels (white) from Tianba Flysch (Scale bar=30 μ m); (b) Enlarged melt inclusion consisting of pyroxene crystals (light grey), residual glass (dark grey), and minor sulfide droplet (bright spot). The pyroxenes are compositionally zoned (Scale bar=10 μ m).

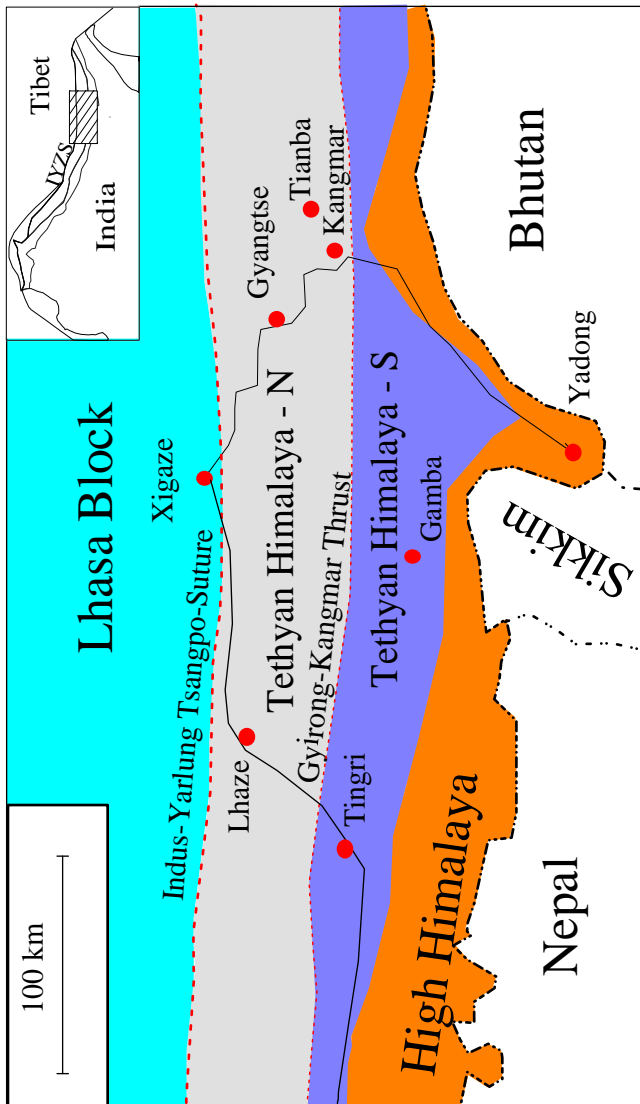
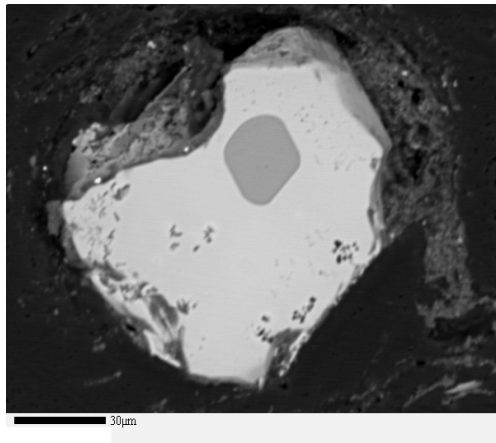
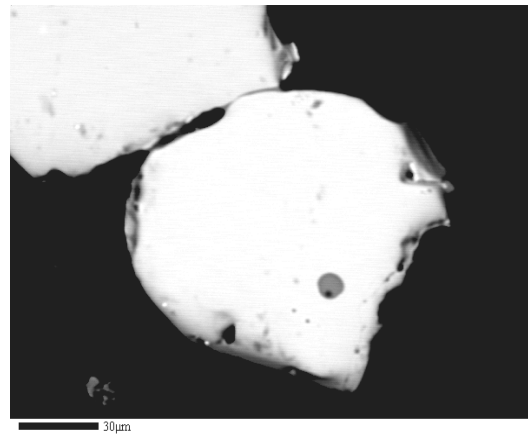


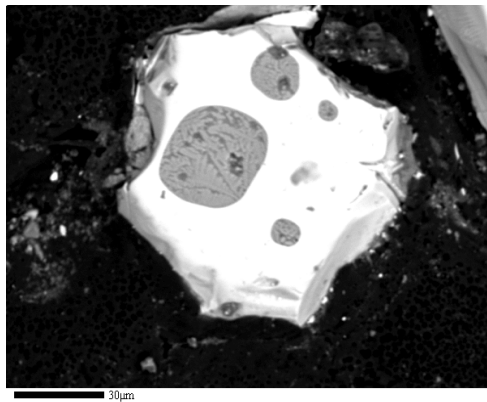
Figure 4.2 Simplified tectonic map of the study area (after Willems et al, 1996). The inset map shows the Tingri-Gyangtse area in the Himalayan system.



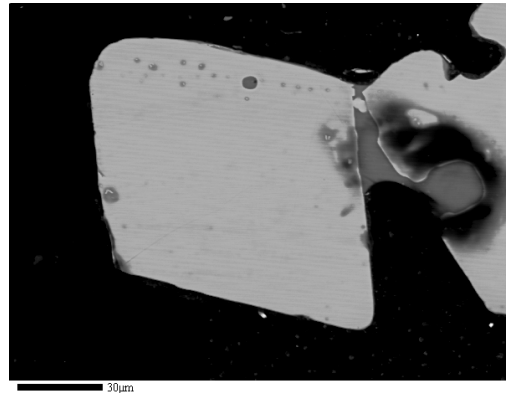
a.



b.



c.



d.

Figure 4.3 Backscattered electron image of melt inclusions (grey) in Cr spinels (white) from Tianba Flysch

(a) Homogenized melt inclusion heated 96 hours at 1250 C.

(b) Homogenized melt inclusion heated 96 hours at 1200 C.

(c) Melt inclusions are randomly distributed in Cr-rich spinel.

(d) Numerous melt inclusions form a band parallel with the outline of an euhedral Cr-rich spinel.

Scale bar=30 μm

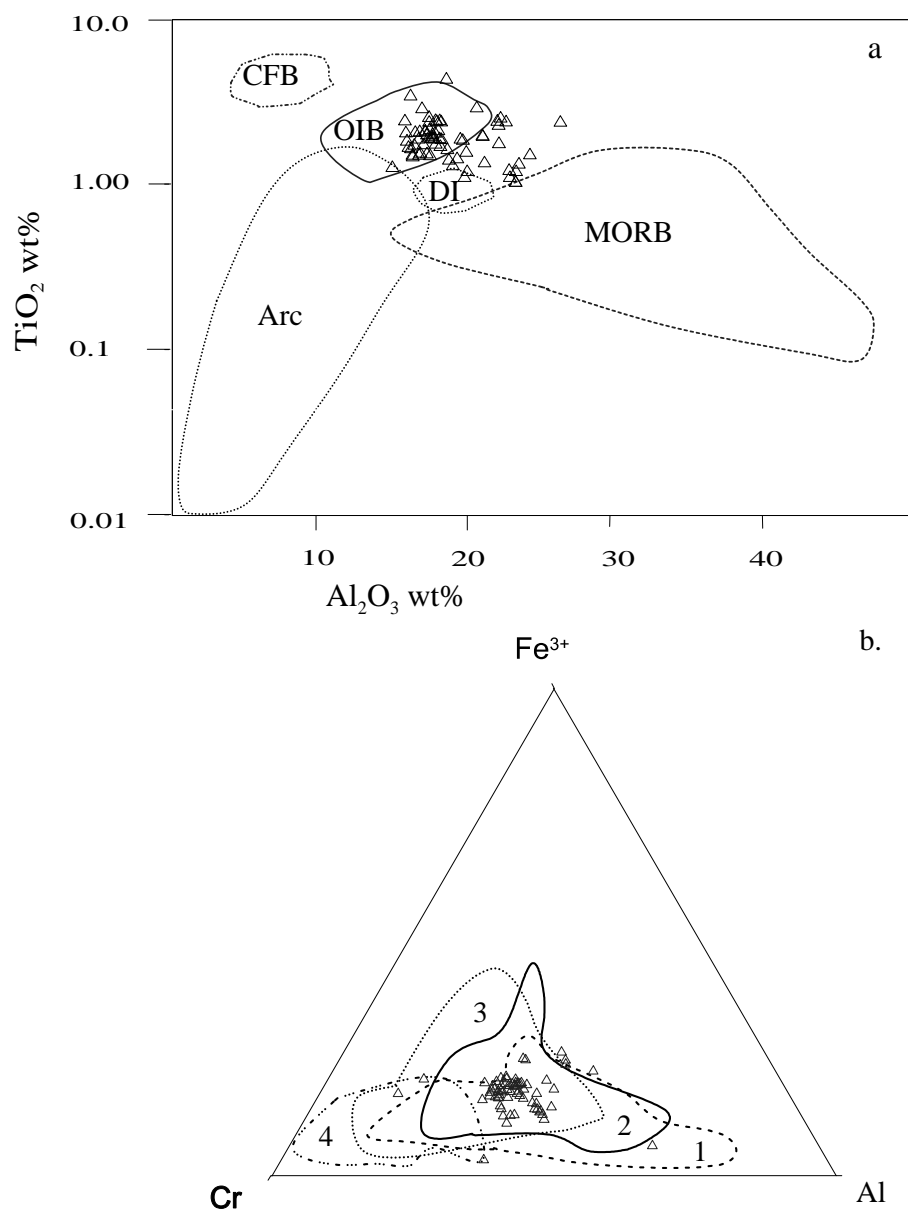


Figure 4.4 Major element contents of spinels and tectonic setting discriminant plots:

a. TiO₂ vs. Al₂O₃ after Kamenetsky et al [14]. Studies of Cr-rich spinel compositions from different tectonic settings show that TiO₂ and Al₂O₃ contents of spinel form a linear trend for those from Continental Flood Basalts (CFB), OIB, DI (Disko Island, W. Greenland), and MORB. Our data mostly plot in the middle of this trend, mainly in the OIB field.

b. Cr-Al-Fe³⁺ ternary plot. 95% of the detrital spinels plot in the 90th percentile contours of OIB field. Different fields are from Barnes and Roeder [33]: 1-MORB; 2-OIB; 3-Island Arc; 4-Boninites.

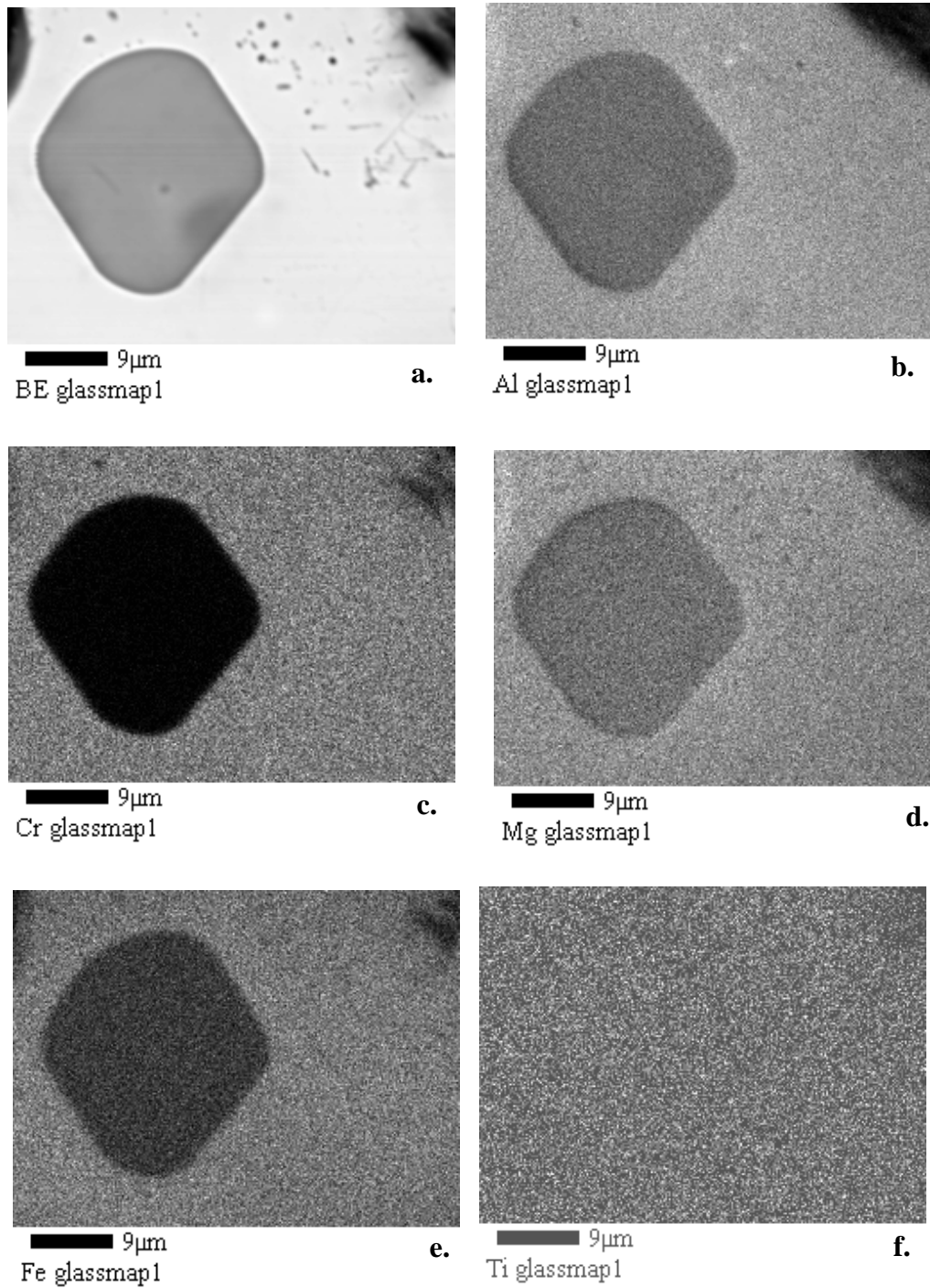


Figure 4.5 Elemental maps of a melt inclusion quenched from 1250C, showing the homogenised melt inclusion.

a. Backscatter image of the melt inclusion; **b.** X-ray image of Al distribution; **c.** X-ray image of Cr distribution; **d.** X-ray image of Mg distribution; **e.** X-ray image of Fe distribution; **f.** X-ray image of Ti distribution.

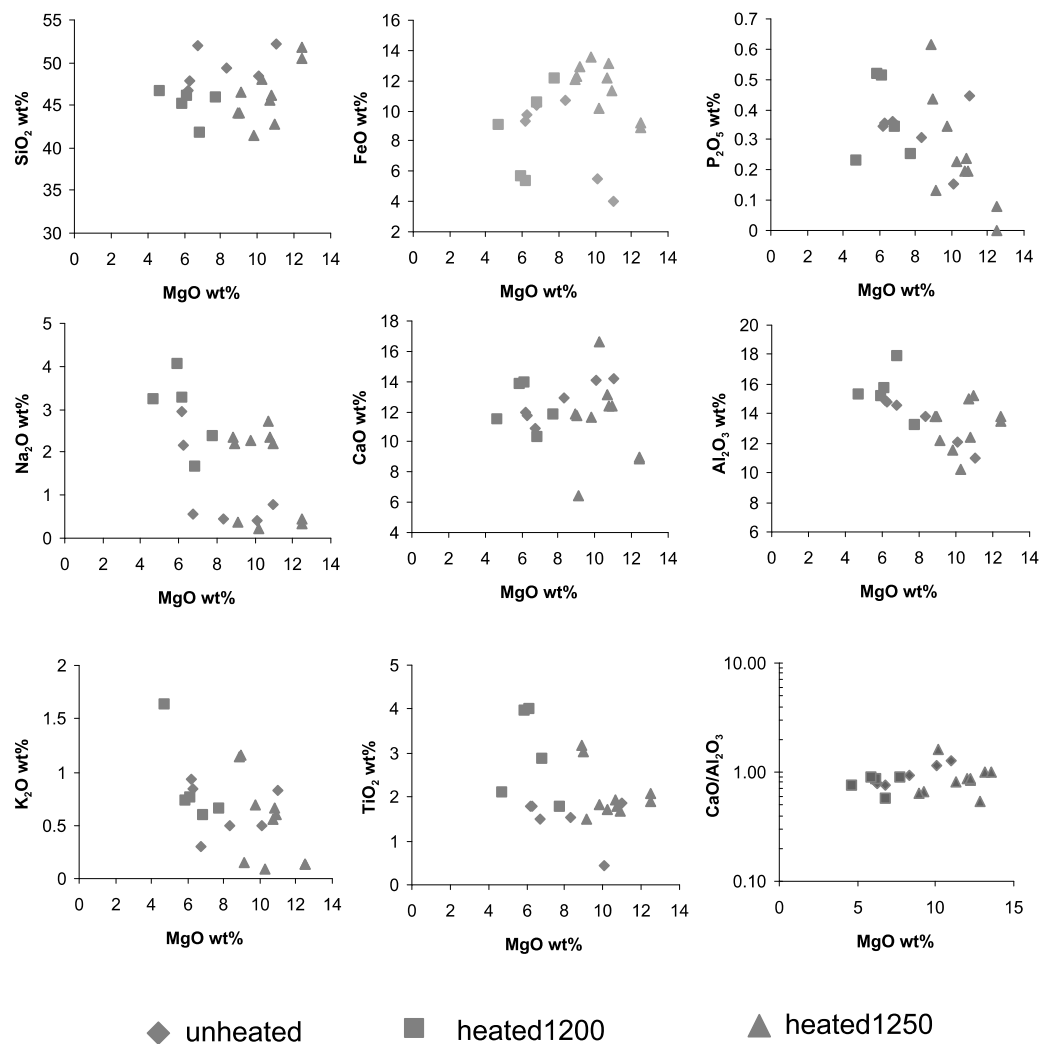


Figure 4.6 Major-element compositions of melt inclusions in the detrital spinels from Tianba Flysch. Note K_2O , TiO_2 , Al_2O_3 , P_2O_5 , and Na_2O are increasing with decreasing MgO , showing relative enrichment of incompatible elements consistent with the crystallization of olivine and spinel.

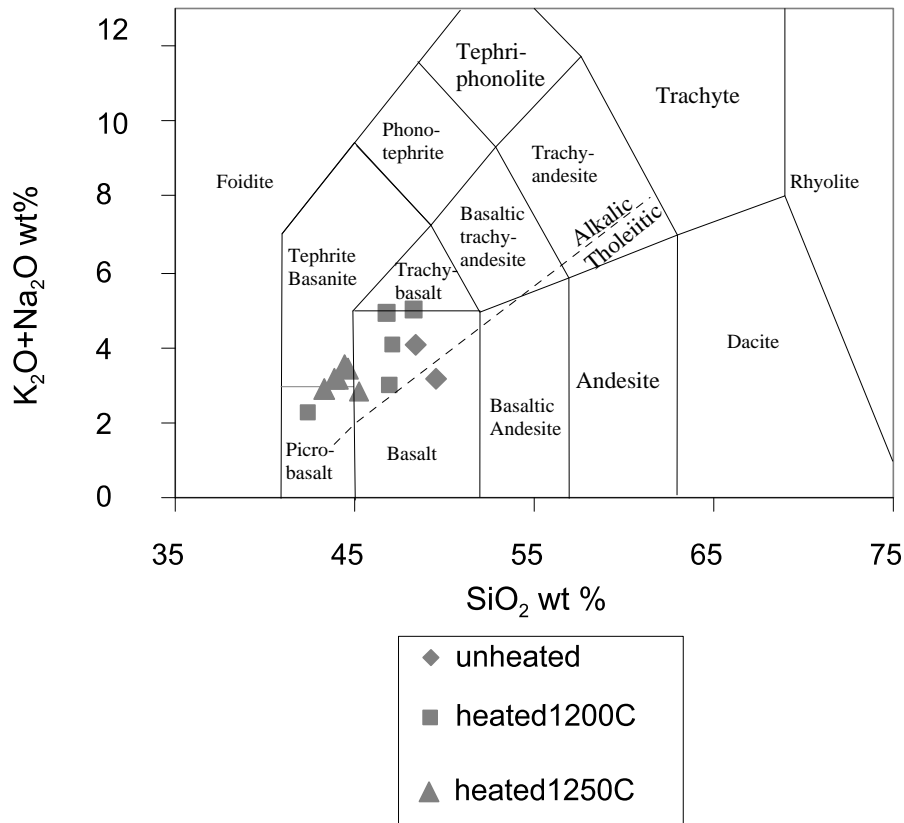


Figure 4.7 Total alkalis vs silica plot after Le Bas et al. [34]. The Macdonald-Katsura line that divides the tholeiitic series from the alkalic series is from Macdonald and Katsura[35]. In our glass data, there are 13 analyses with Na₂O content >1 wt%, and only one plots in the tholeiitic area, hence the parental magma of these melt inclusions must be alkali basalt.

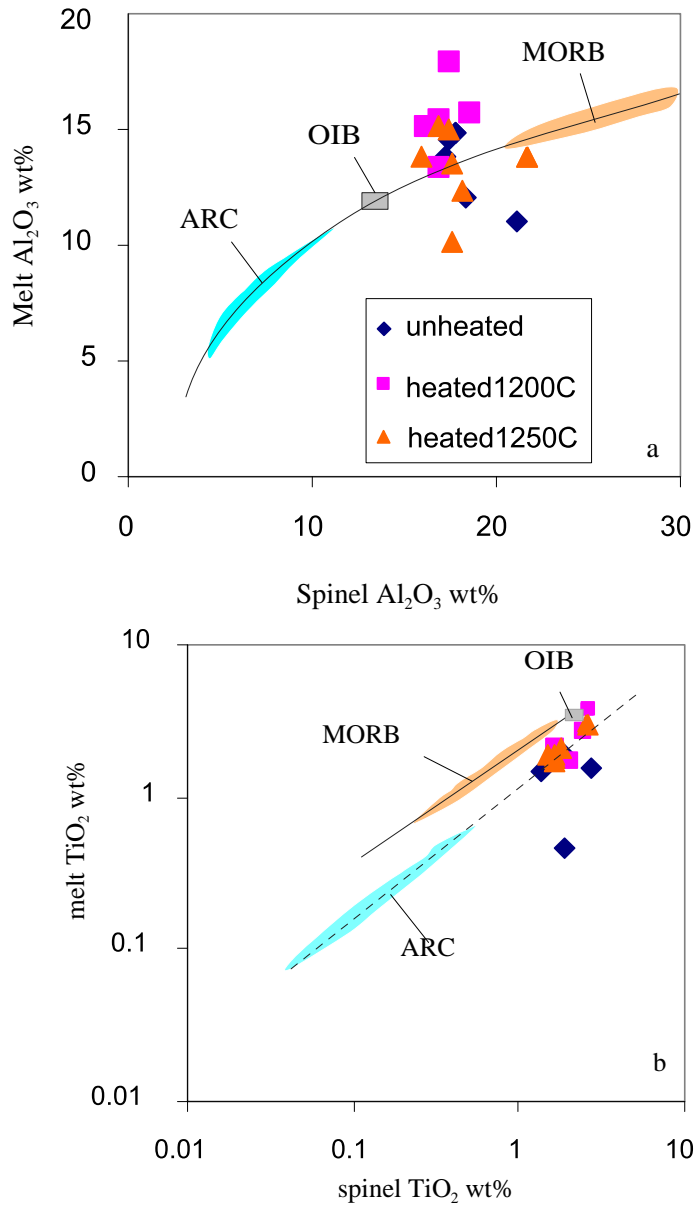


Figure 4.8 Positive correlation between Al_2O_3 and TiO_2 contents in melt inclusions and hosted spinels (the best fit lines and fields are from Kamenetsky et al., 2000). Continuous line in **a.** is a power law best fit through published data; Continuous and dashed lines in **b.** are best fit through the high-Al (Al_2O_3 in melt >14 wt%) and low Al (Al_2O_3 in melt <14 wt%) data, respectively. Our data are either close to, or aligned with their best fit lines. The relatively narrow range of our data and proximity to the OIB point suggest a single tectonic provenance for these detrital spinels.

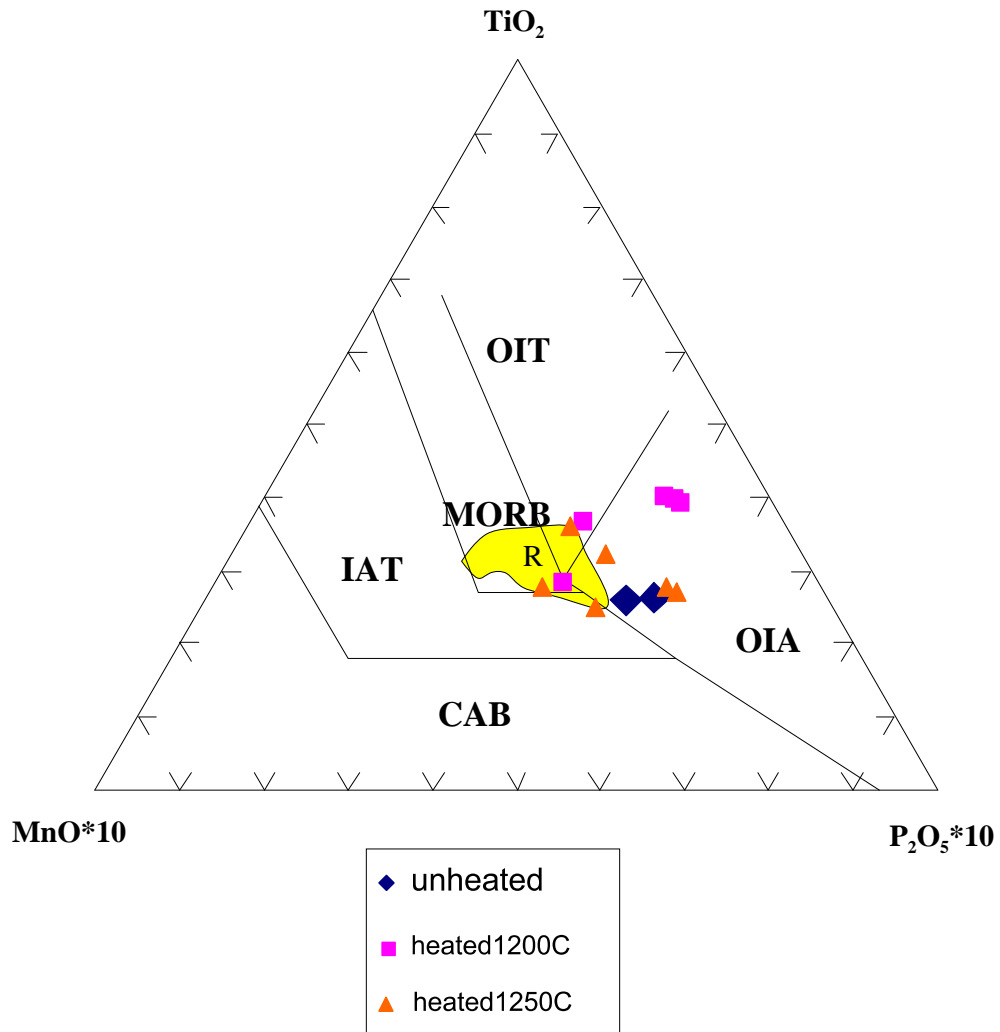


Figure 4.9 TiO_2 - MnO - P_2O_5 plot (after Mullen, 1983). CAB: Calc-Alkaline basalts; IAT: Island Arc Tholeiites; OIA: Ocean Island Alkali basalt or Seamount Alkali Basalt; OIT: Ocean Island Tholeiites. 13 of data ($\text{Na}_2\text{O} > 1$ wt%) plot in, or very close to, the OIA field. Therefore the melt of the spinel melt inclusions was most like oceanic island basalt. R represents the field of Rajmahal Traps (data from Storey et al., 1992).

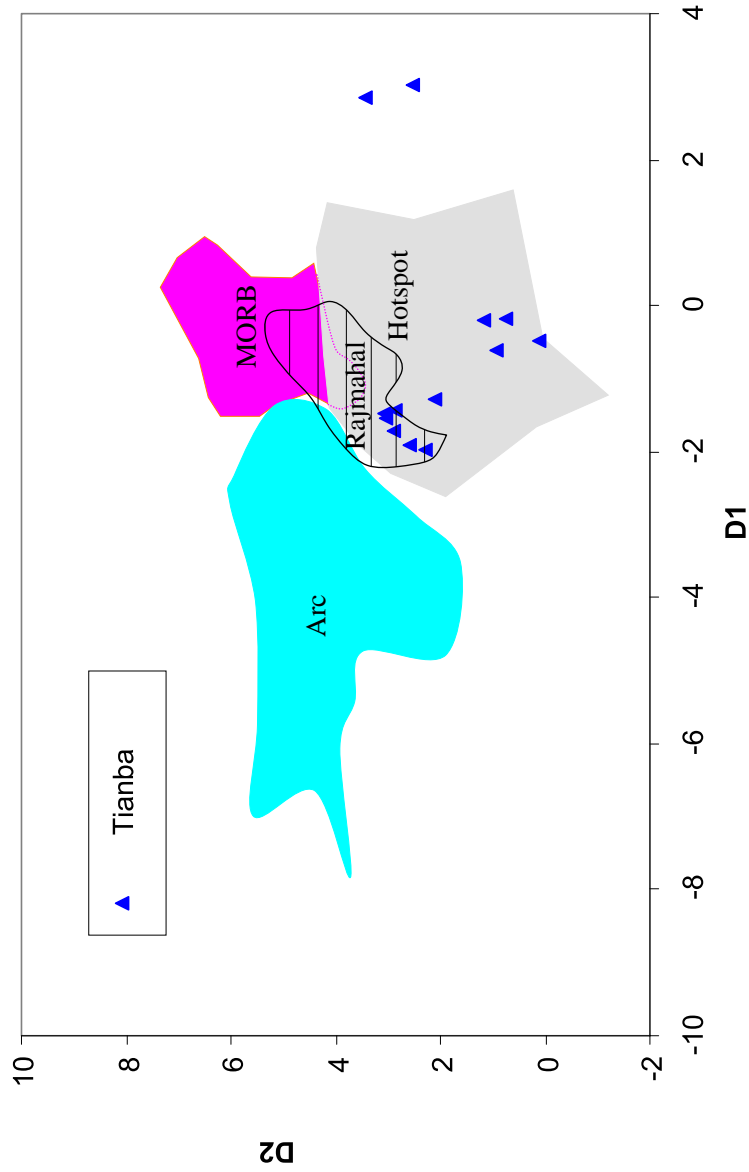


Figure 4.10 Discriminant function plot of basalt from three tectonic settings. The compositions of basalt (SiO₂:40-55 wt%) from Izu Island Arc (50), Andean Arc(50), Mariana Arc (50), Honshu Arc(50), MORB(200), Hawaii(50), Iceland(50), Kerguelen Island (50), and Canary Island (50) are used to develop this plot using linear discriminant function(Iida) in Splus [29]. 11 of 13 melt inclusions in Tianba Flysch plot in Hotspot basalt field, and no points plot in arc field. Rajmahal data from Kent et al., 1997; Storey et al., 1992.

$$D1 = 2.02 \cdot \log(\text{SiO}_2/\text{TiO}_2) - 2.15 \cdot \log(\text{Al}_2\text{O}_3/\text{TiO}_2) - 3.14 \cdot \log(\text{FeO}/\text{TiO}_2) + 0.82 \cdot \log(\text{CaO}/\text{TiO}_2) + 0.41 \cdot \log(\text{MgO}/\text{TiO}_2) - 1.07 \cdot \log(\text{K}_2\text{O}/\text{TiO}_2) - 0.37 \cdot \log(\text{Na}_2\text{O}/\text{TiO}_2) + 0.53 \cdot \log(\text{P}_2\text{O}_5/\text{TiO}_2)$$

$$D2 = 1.69 \cdot \log(\text{SiO}_2/\text{TiO}_2) - 2.88 \cdot \log(\text{Al}_2\text{O}_3/\text{TiO}_2) - 0.09 \cdot \log(\text{FeO}/\text{TiO}_2) + 0.85 \cdot \log(\text{CaO}/\text{TiO}_2) - 0.49 \cdot \log(\text{MgO}/\text{TiO}_2) - 1.15 \cdot \log(\text{K}_2\text{O}/\text{TiO}_2) + 3.48 \cdot \log(\text{Na}_2\text{O}/\text{TiO}_2) - 0.17 \cdot \log(\text{P}_2\text{O}_5/\text{TiO}_2)$$

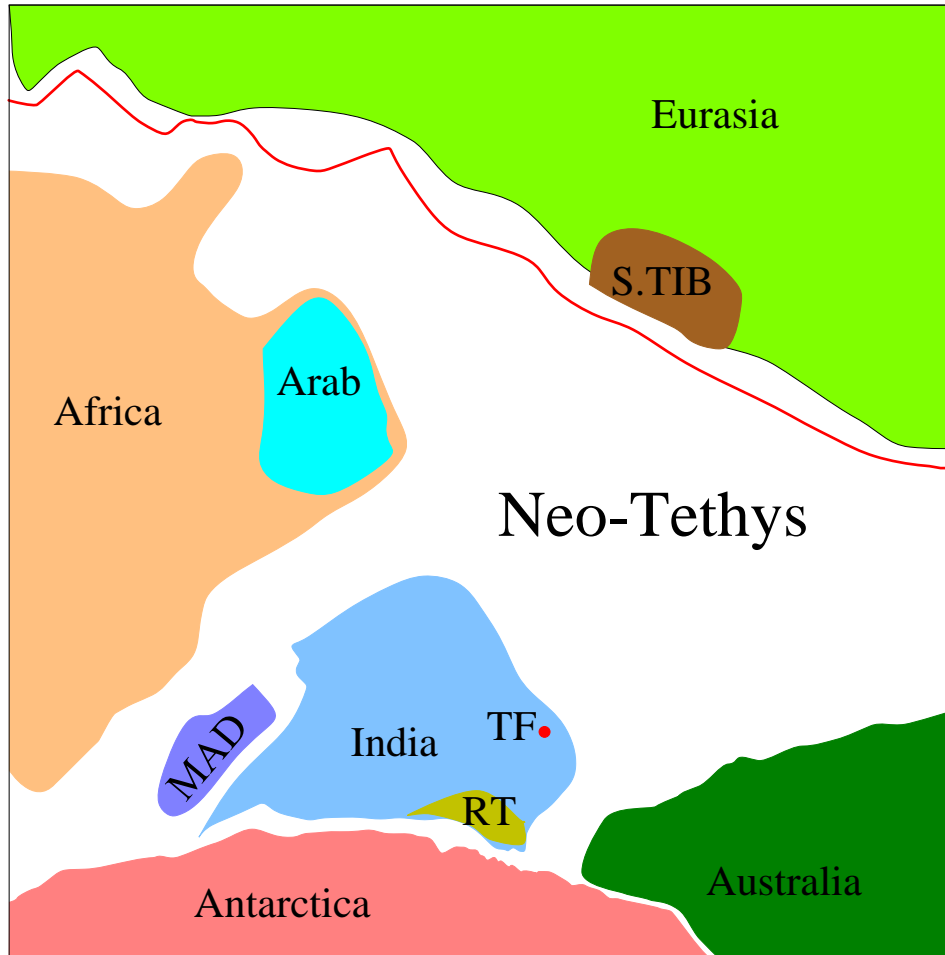


Figure 4.11 Reconstruction map at about 117 Ma (modified after Besse and Courtillot, 1988). MAD, Madagascar block; S.TIB, southern Tibet; RT, Rajmahal Traps; TF, Tianba Flysch. The red line is the major subduction zone.

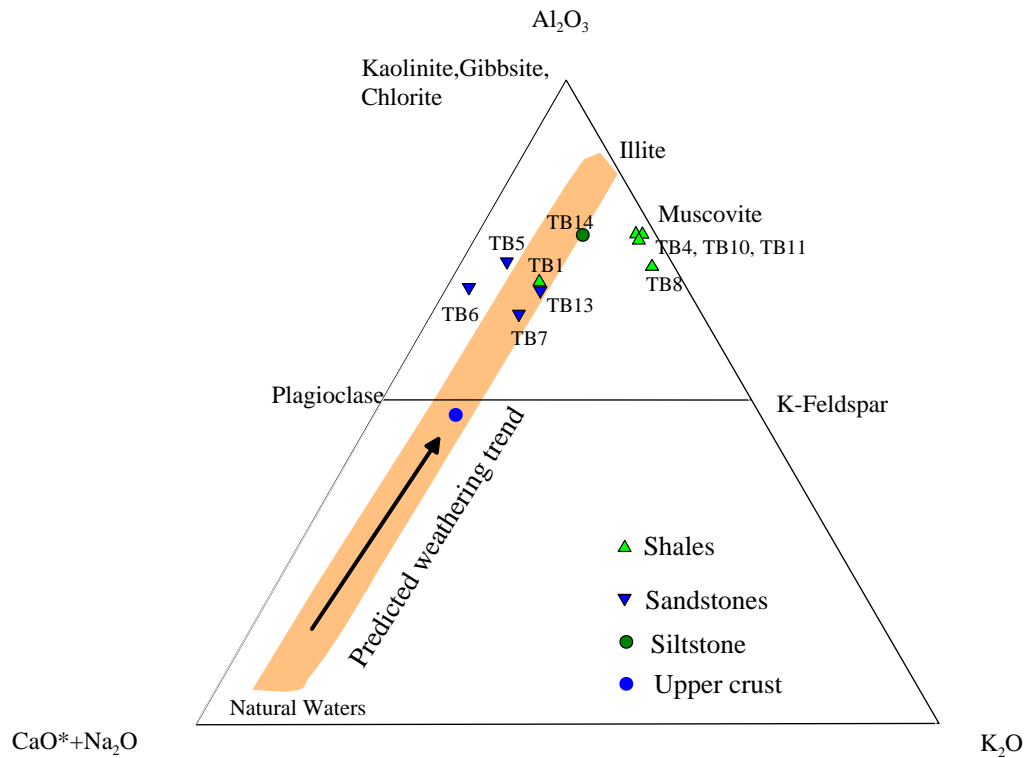


Figure 5.1 CIA ternary plot of the Tianba Flysch. Modified after Bock et al. (1998). The enrichment in Al_2O_3 and depletion of $CaO+Na_2O+K_2O$ reflect the degree of chemical weathering to which the materials have been subjected. Four analyses (TB1, TB7, TB13, TB14) defined a linear trend encompassed in the predicted weathering trend for the average upper crustal composition. Four shales do not follow the predicted weathering trend, indicating processes in addition to the weathering have affected these sediments. TB6 and TB5 plot close to the Al_2O_3 - $CaO+Na_2O$ join, which may indicate a significant volcanic input.

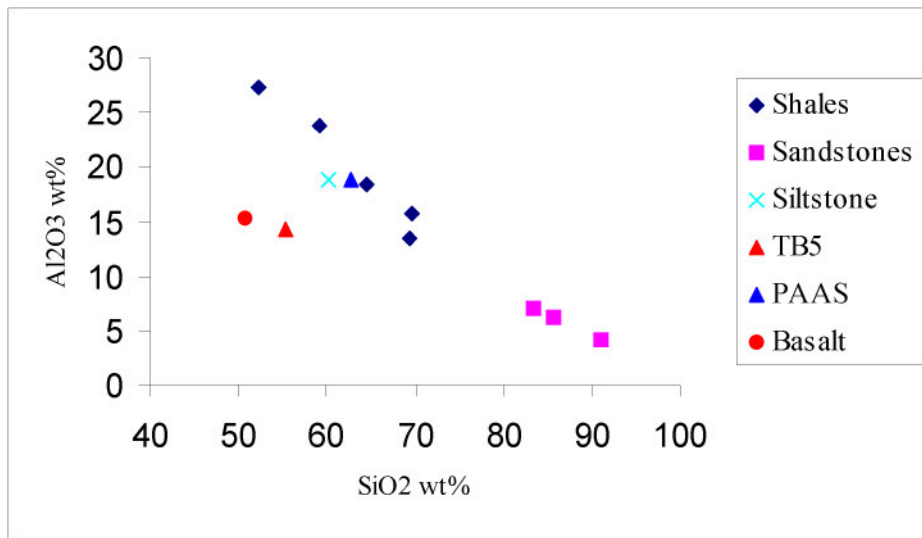


Figure 5.2 SiO₂-Al₂O₃ plot of the Tianba Flysch. TB5 (based on CaO and LOI-free recalculation) is not in the linear trend formed by the rest of analyses in Tianba Flysch.

PAAS from Taylor and McLennan (1985), average basalt composition from Condie (1993).

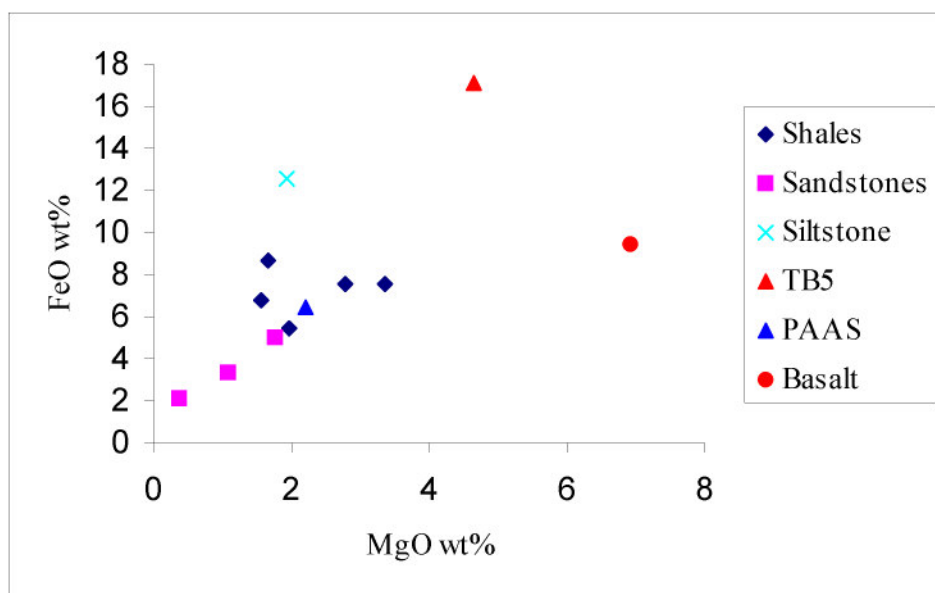


Figure 5.3 MgO-FeO plot of the Tianba Flysch. TB14 (siltstone) has high Fe content falling off the Fe-Mg trend of the other analyses. PAAS from Taylor and McLennan (1985), basalt from Condie (1993).

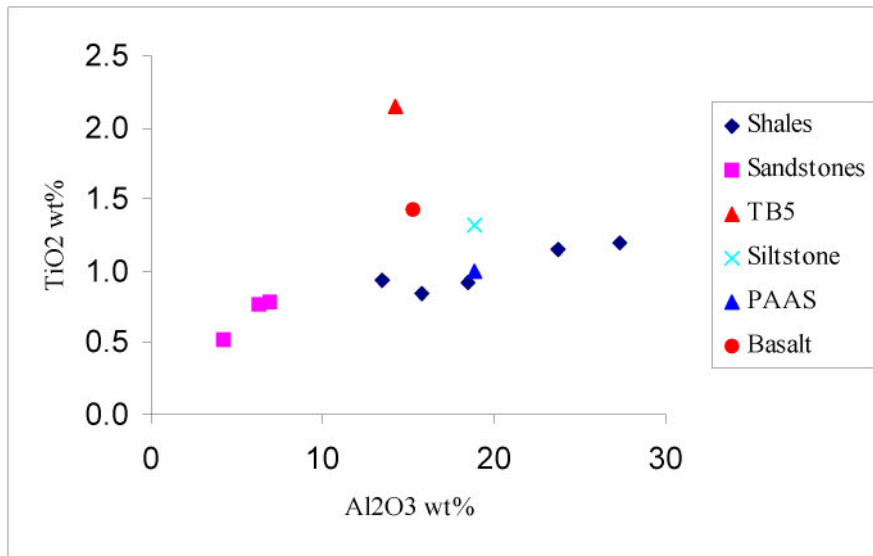


Figure 5.4 Al₂O₃-TiO₂ plot of the Tianba Flysch. There is an approximate linear relationship between Al₂O₃ and TiO₂ in the analyses from the Tianba Flysch. PAAS from Taylor and McLennan (1985), basalt from Condie (1993).

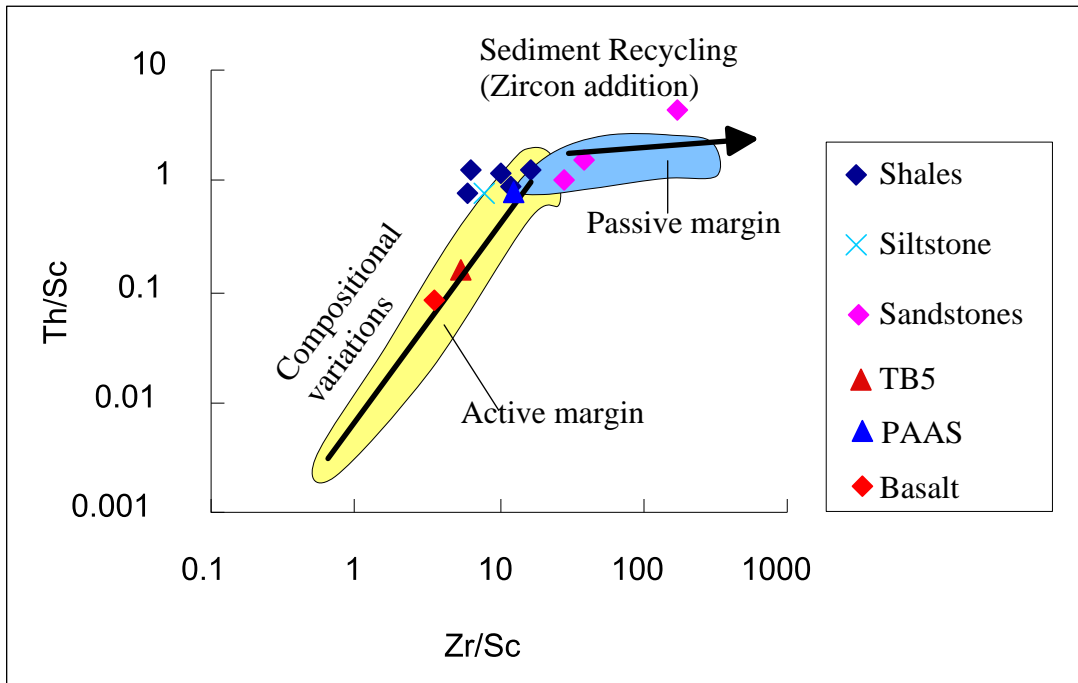


Figure 5.5 Th/Sc-Zr/Sc plot of the Tianba Flysch. Passive margin and Active margin fields, and trends of compositional variations and sediment recycling are from McLennan et al. 1990. PAAS from Taylor and McLennan (1985), average basalt composition from Condie (1993). There is a significant enrichment of Zircon (high Zr/Sc) in passive margin setting resulting from sedimentary sorting and recycling.

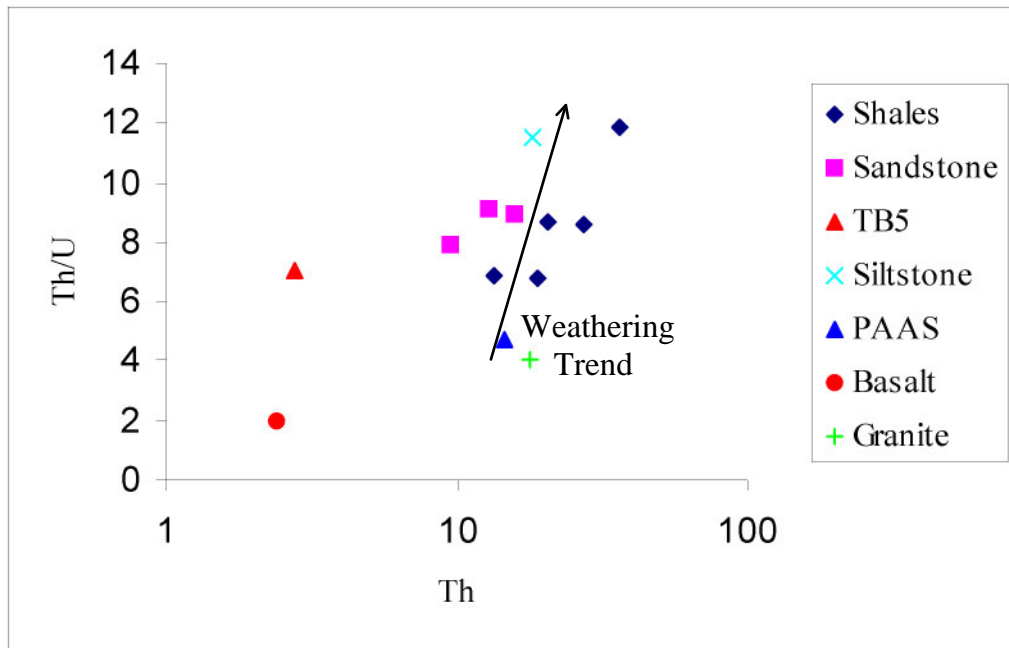


Figure 5.6 Th/U-Th plot of the Tianba Flysch. Arrow indicates a weathering trend. Note analyses (except TB5) from the Tianba Flysch follow the weathering trend, similar to Australian Shales with cratonic provenance (McLennan et al., 1990). PAAS from Taylor and McLennan (1985), average basalt and granite compositions from Condie (1993).

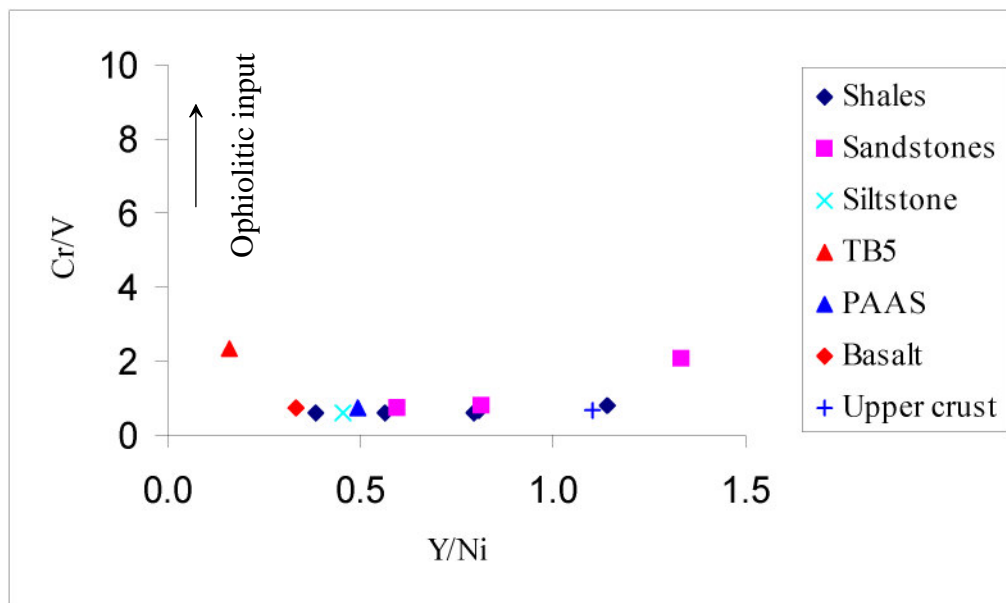


Figure 5.7 Cr/V-Y/Ni plot of the Tianba Flysch.

Note Cr/V ratios of the Tianba Flysch are constantly low with the increase in Y/Ni ratios. Mafic-ultramafic sources tend to have high Fe, Cr, Ni abundances with low Y/Ni and high Cr/V ratios. TB5 has high Cr and Ni abundances indicating a volcanic provenance. PAAS and Upper Crust from Taylor and McLennan (1985), average basalt composition from Condie (1993).

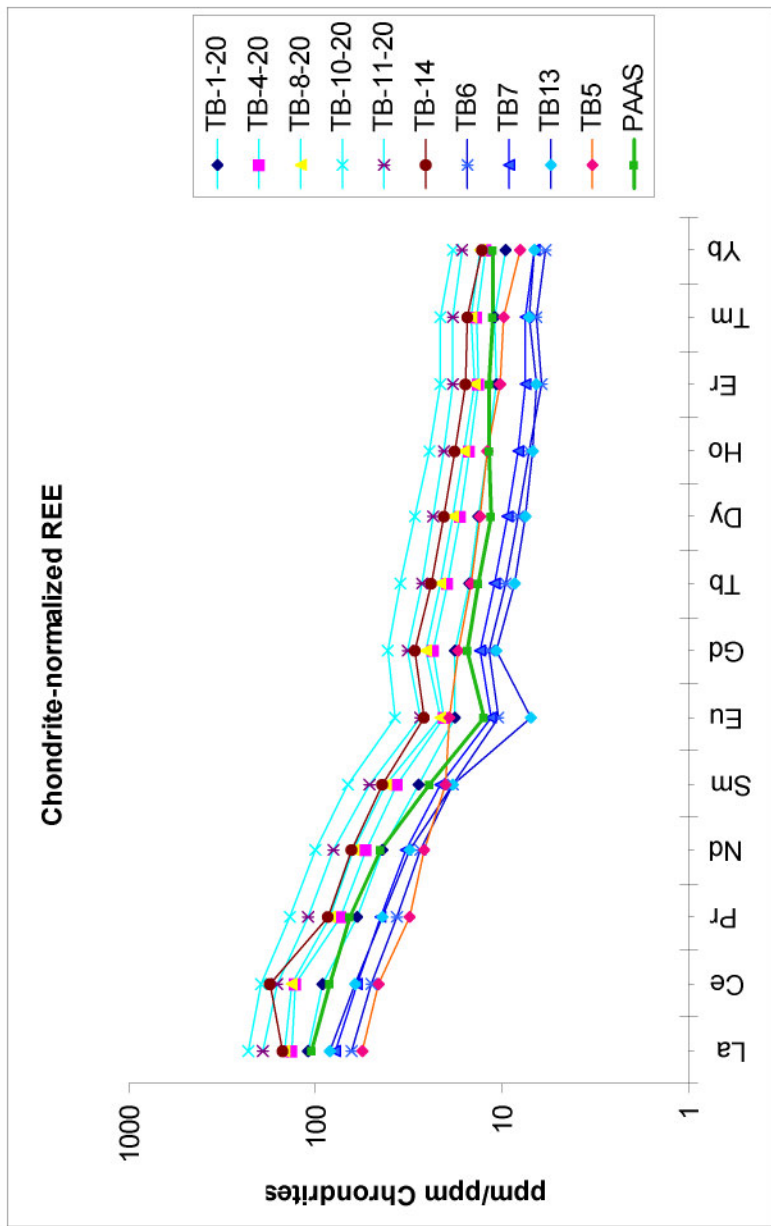


Figure 5.8 Chondrite-normalized REE plot of the Tianba Flysch, north of Tianba village. All analyses except TB5 show LREE enrichments and negative Eu anomalies, similar to PAAS, indicating a common cratonic provenance. Relatively flatten REE trend of TB5 points to a significant volcanic source. PAAS from Taylor and McLennan (1985).

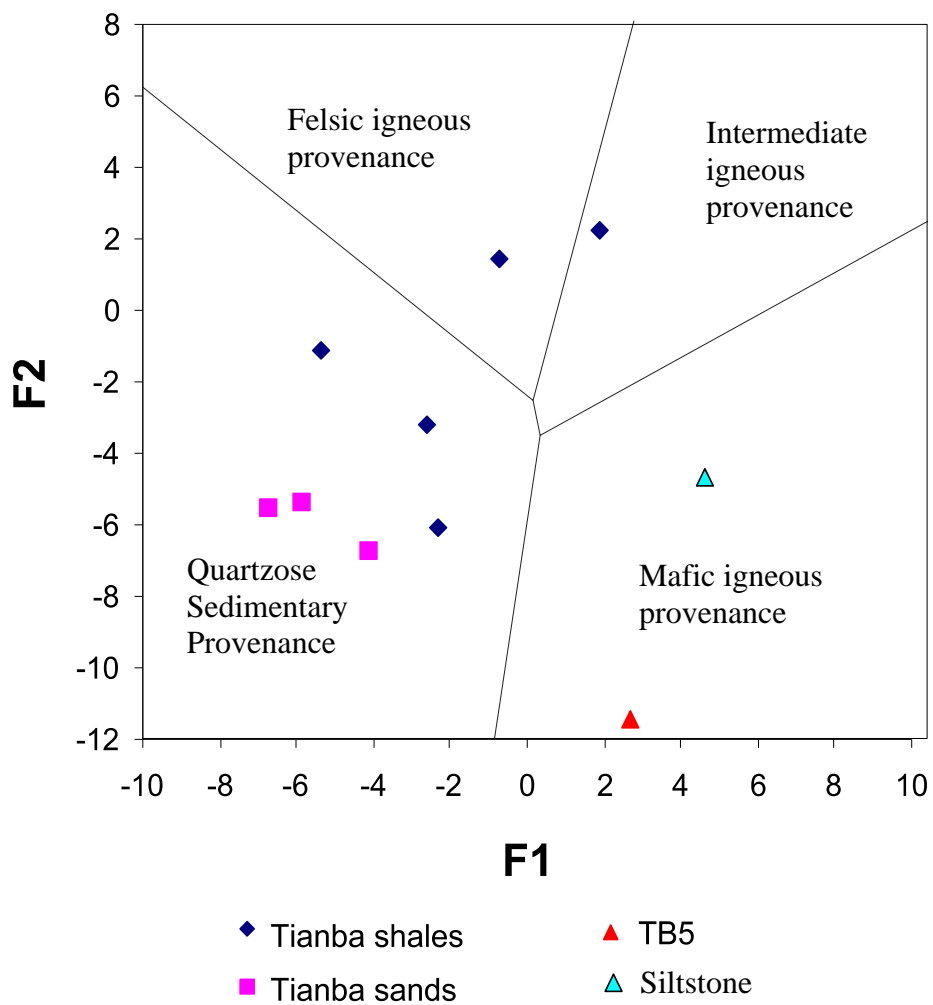


Figure 5.9 Tectonic discriminant diagram for the Tianba Flysch. Tectonic setting fields are from Roser and Korsch (1988).
 $F1 = -1.773TiO_2 + 0.607Al_2O_3 + 0.76Fe_2O_3 - 1.5MgO + 0.616CaO + 0.509Na_2O - 1.224K_2O - 9.09$
 $F2 = 0.445TiO_2 + 0.07Al_2O_3 - 0.25Fe_2O_3 - 1.142MgO + 0.438CaO + 1.475Na_2O + 1.426K_2O - 6.86$
 Data from Roser and Korsch (1988).

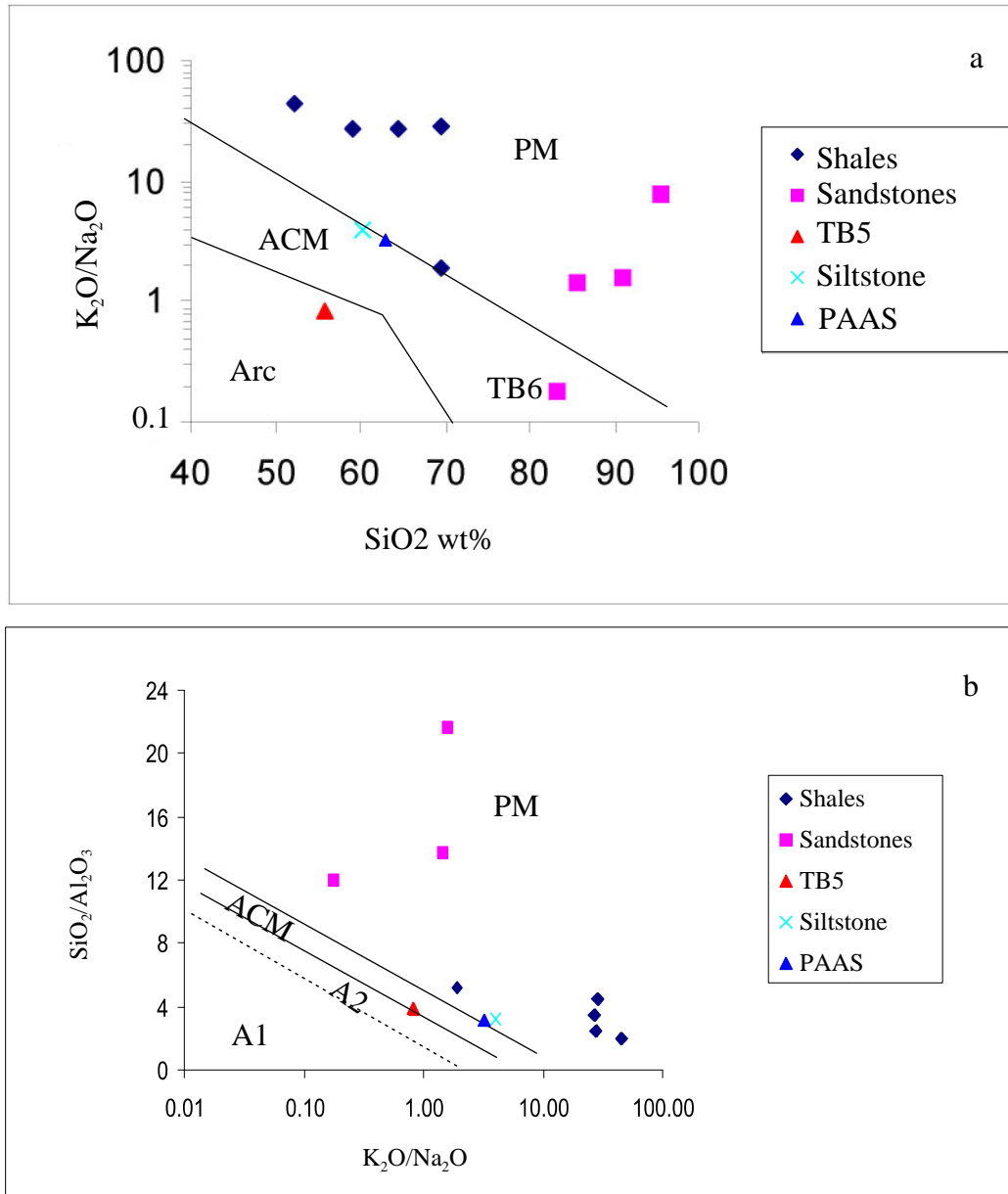


Figure 5.10 K_2O/Na_2O - SiO_2 (a) and SiO_2/Al_2O_3 - K_2O/Na_2O (b) plots of the Tianba Flysch.

Tectonic setting: PM-passive margin, ACM-active continental margin, ARC-volcanic arc, A1-Arc setting, A2-evolved arc setting (from Roser and Korsch, 1986). Most samples from the Tianba Flysch plot in the passive margin area while TB5 plots in arc or active continental margin, indicating a volcanic source for the upper Tianba Flysch. PAAS from Taylor and McLennan (1985).

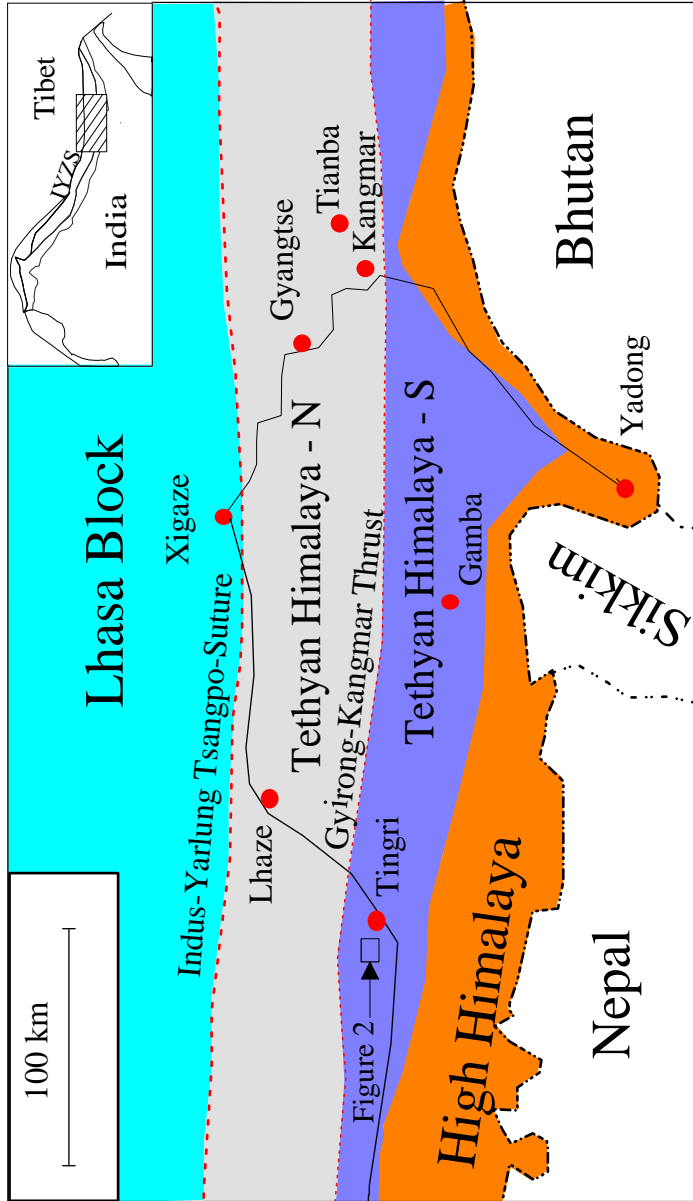


Figure 6.1 Sketch geologic map of Tingri region, southern Tibet. The inset map shows this region located in the Himalayan system. Modified after Willems et al.(1996).

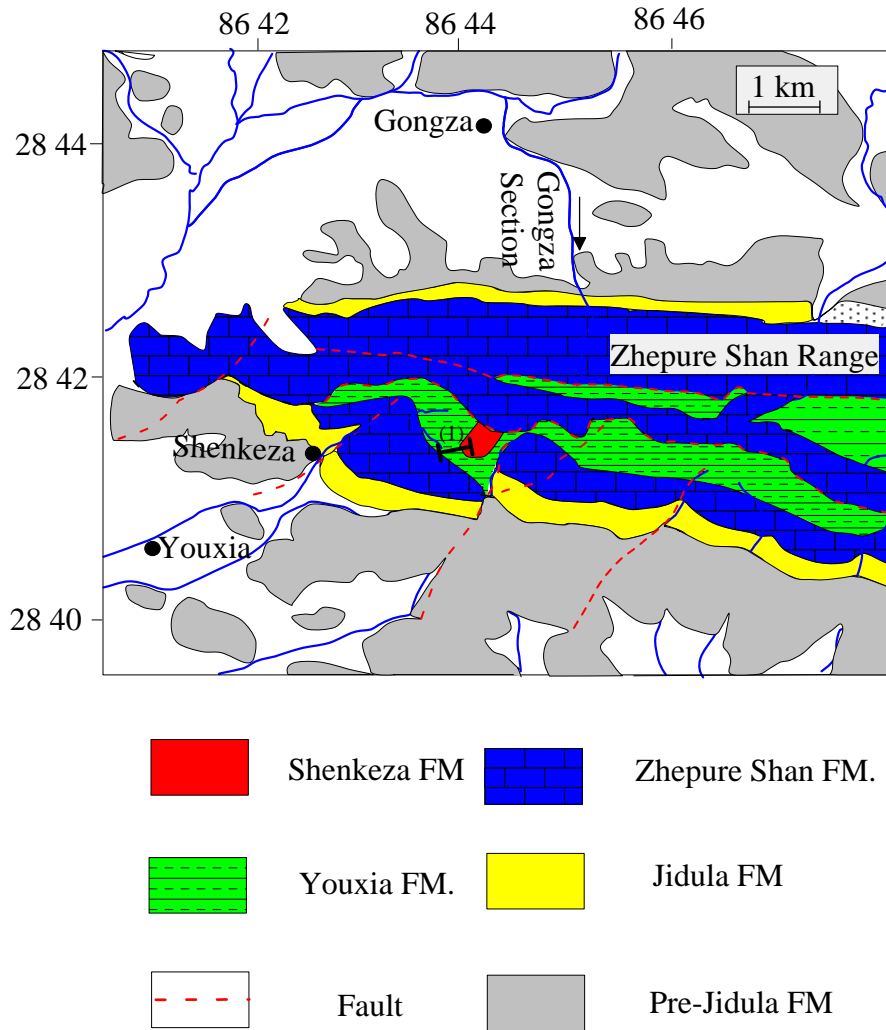


Figure 6.2 Simplified geologic map showing the location of the studied sections in the Tingri region on the western flank of Zhepure Shan Mountain. Note: (1) is measured section at Shekeza. Geographic coordinates in degrees, minutes.

Gongza Section

Shenkeza Section

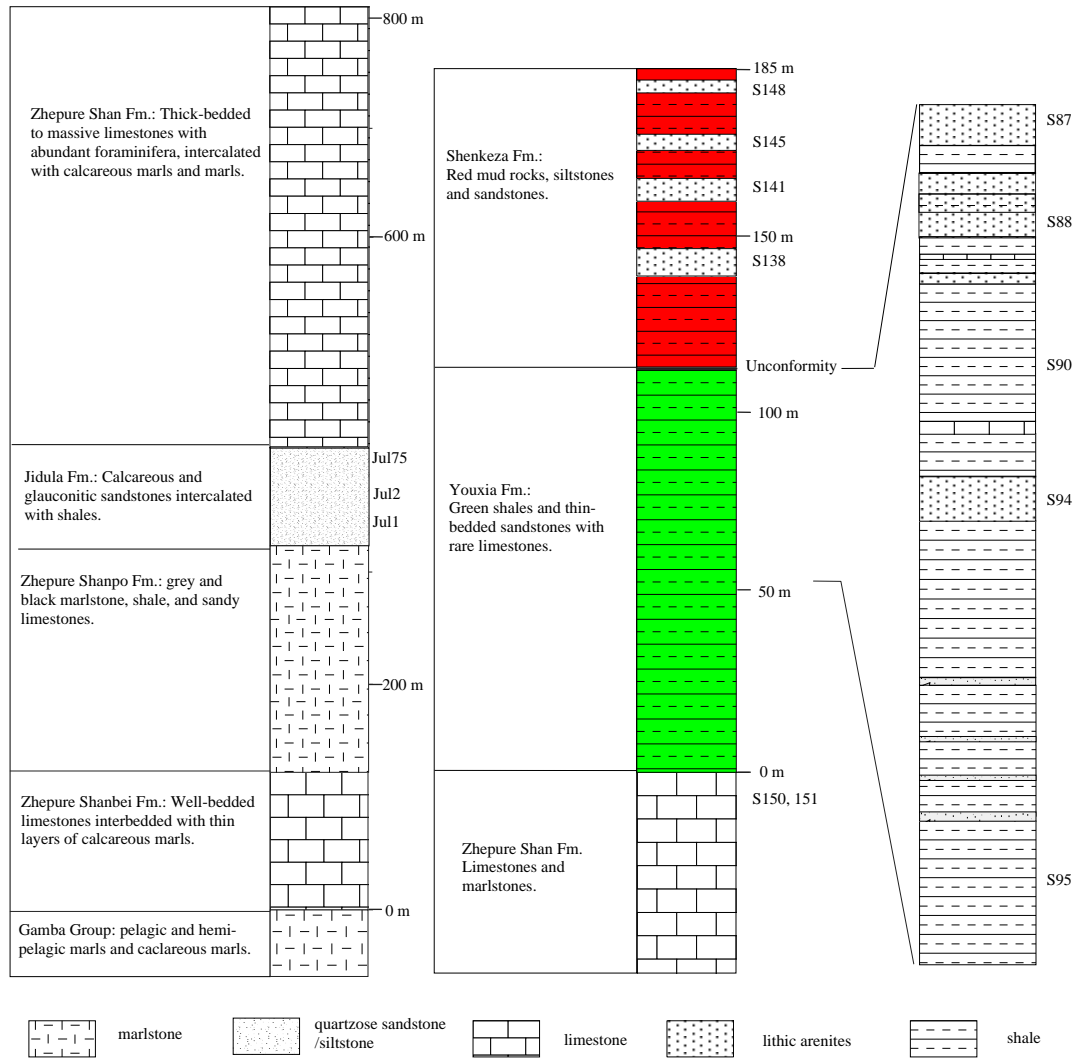


Figure 6.3 Stratigraphic columns of lower Tertiary sequence in the Tingri region. The Shenkeza section was measured by us in 2000, and the Gongza section is from Willems et al. (1996).

Section locations are shown in Figure 2. Sample locations are indicated by "Sxxx" at Shenkeza section and "Julxxx" at Gongza section.



Figure 6.4 View to E of the upper part of the Youxia Formation in the head of the Shenkeza valley, made up of green shales and sandstones. The shales conformably overlie the Zhepure Shan limestones. The section of the upper Youxia Formation was measured up the gully on the left side of the photo.



Figure 6.5 View to N of Shenkeza Formation of red shales and occasional intercalations of fine-grained sandstones. The Zhepure Shan limestones above are in thrust contact with this unit.

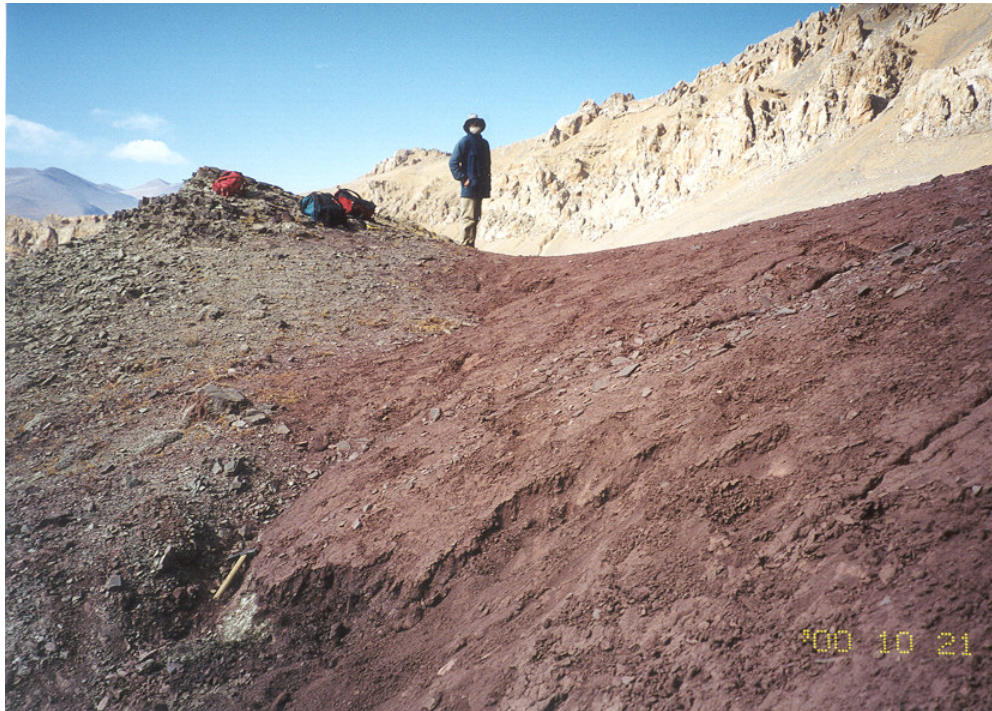
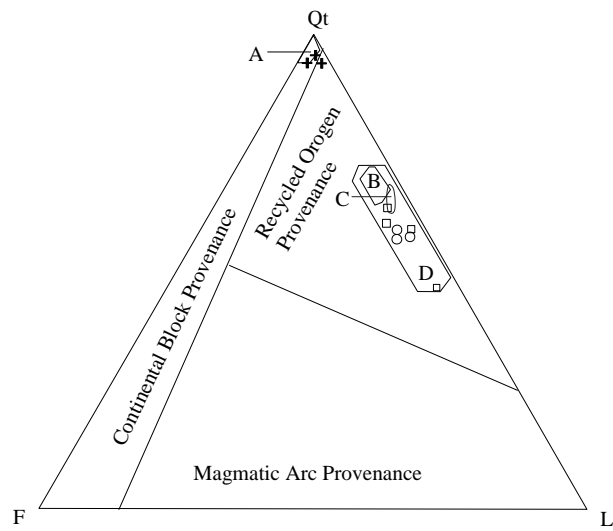


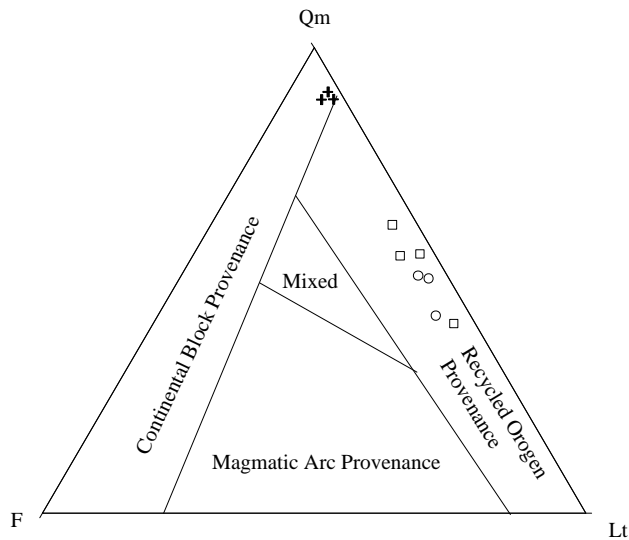
Figure 6.6 View to NW of the unconformity between the Youxia and Shenkeza Formations. Note there is abrupt change in color from green to red. Excavation of the contact at the location of the hammer in this photo revealed a 1 m thick soil horizon of the base of the red unit, and a rubbly regolith of green sandstone fragments below it. [Professor W. Kidd stands on the unconformity, 21 Oct 2000]



Figure 6.7 Hummocky cross-stratification in the top sandstones of the Youxia Formation, indicating a depositional environment of storm waves during the late Youxia Formation.



- A Stumpata/Dibling
- B Balakot Fm.
- C Subathu Fm.
- D Siwalik (Nepal)



- + Jidula Sandstone
- Youxia Green Sandstone
- Shenkeza Red Sandstone

Figure 6.8 Detrital mode plot of lower Tertiary sandstones in the Tingri region Tectonic fields from Dickinson, 1985. Fields of other related Himalayan sandstones shown are from Garzanti et al. (1996)

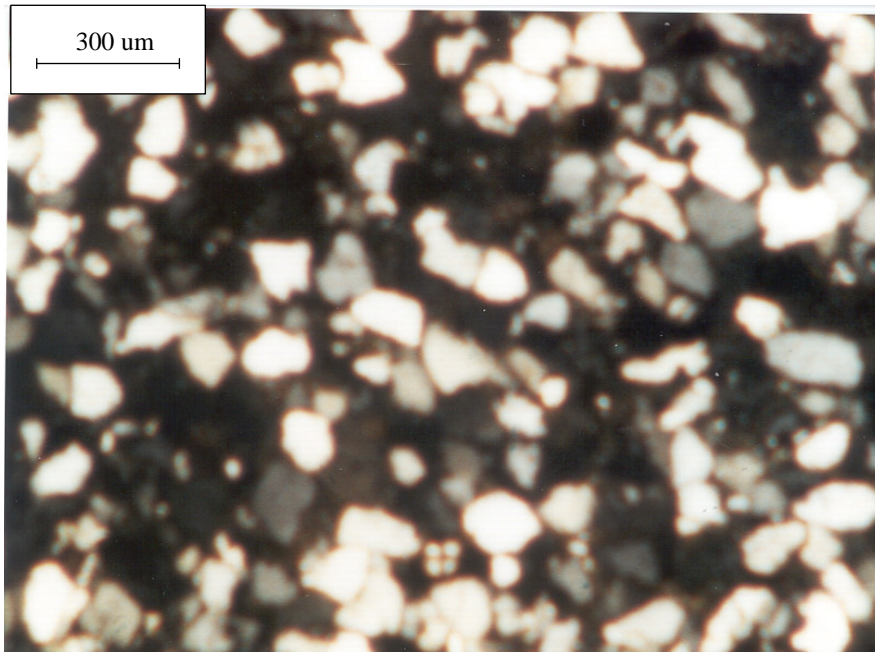


Figure 6.9 Photomicrograph (crossed polars) of quartz-rich sandstone (Jul2) in the Jidula Formation, Gongza section. Note: most quartz grains are well-sorted, unit extinguishing.

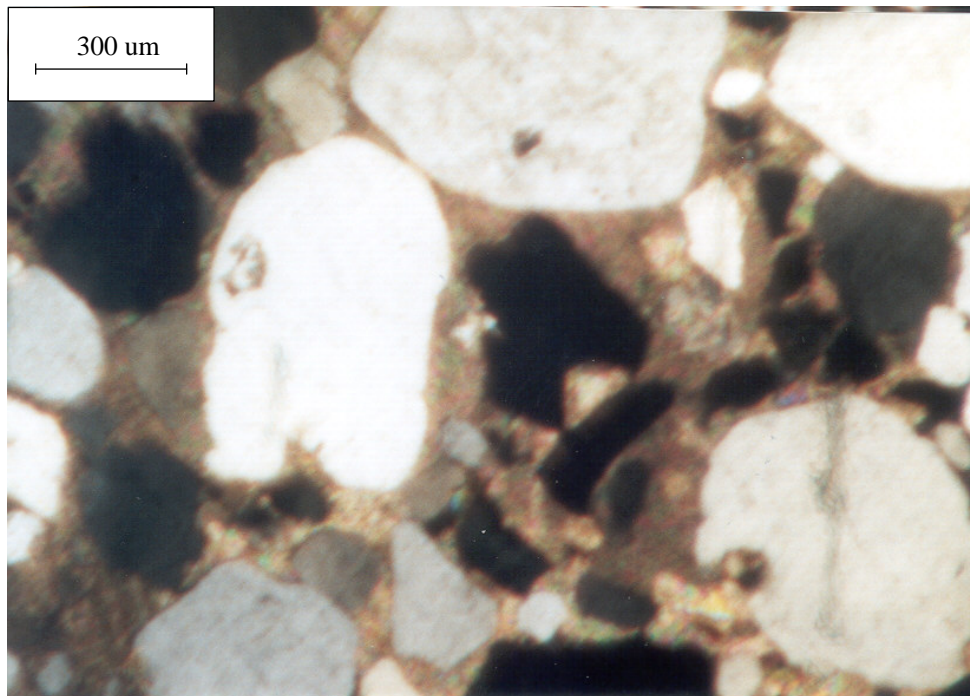


Figure 6.10 Photomicrograph of well-rounded monocrystalline quartz grains with calcite cement in the Jul 75 sandstone of Jidula Formation, Gongza Formation. Opaque minerals are magnetite or ilmenite.

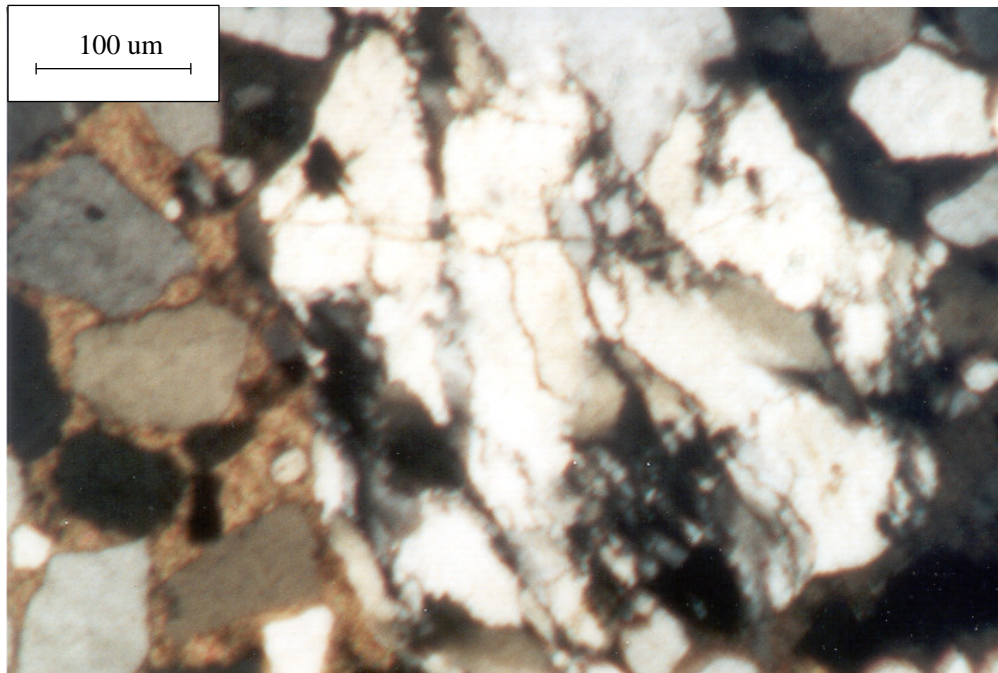


Figure 6.11 Photomicrograph (crossed polars) of a metamorphic rock fragment in Jul 75 sandstone of Jidula Formation, Gongza section.

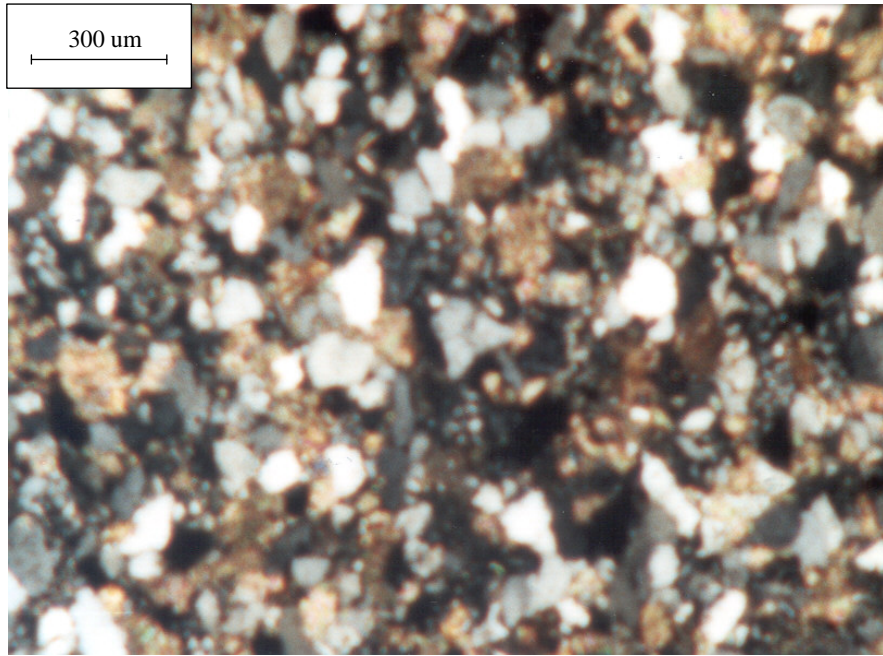


Figure 6.12 Photomicrograph (crossed polars) of lithic-rich sandstone (Shen88) in the Youxia Formation, Shenkeza section. Note most quartz grains are angular in shape.

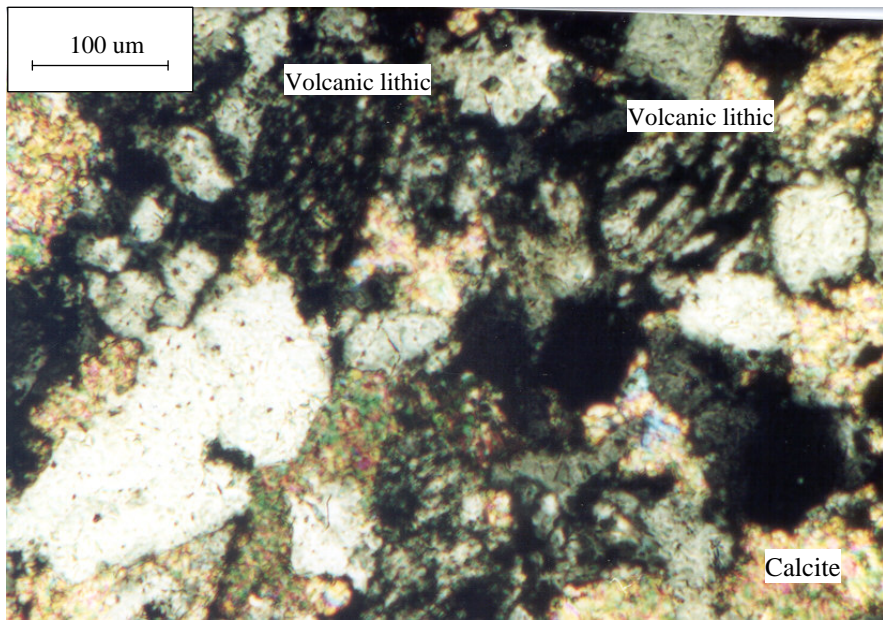


Figure 6.13 Photomicrograph (crossed polars) of volcanic rock fragments in the Shen88 sandstone of the Youxia Formation, Shenkeza section.

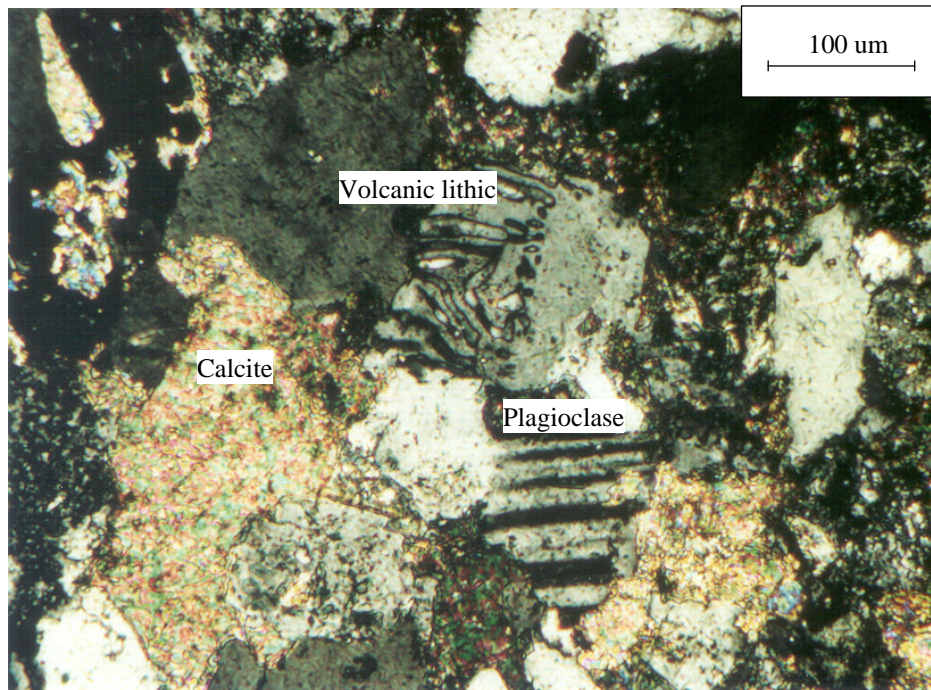


Figure 6.14 Photomicrograph (crossed polars) of Shen94 sandstone in the Youxia Formation, Shenkeza section. Note there are calcite, volcanic lithic and plagioclase grains.

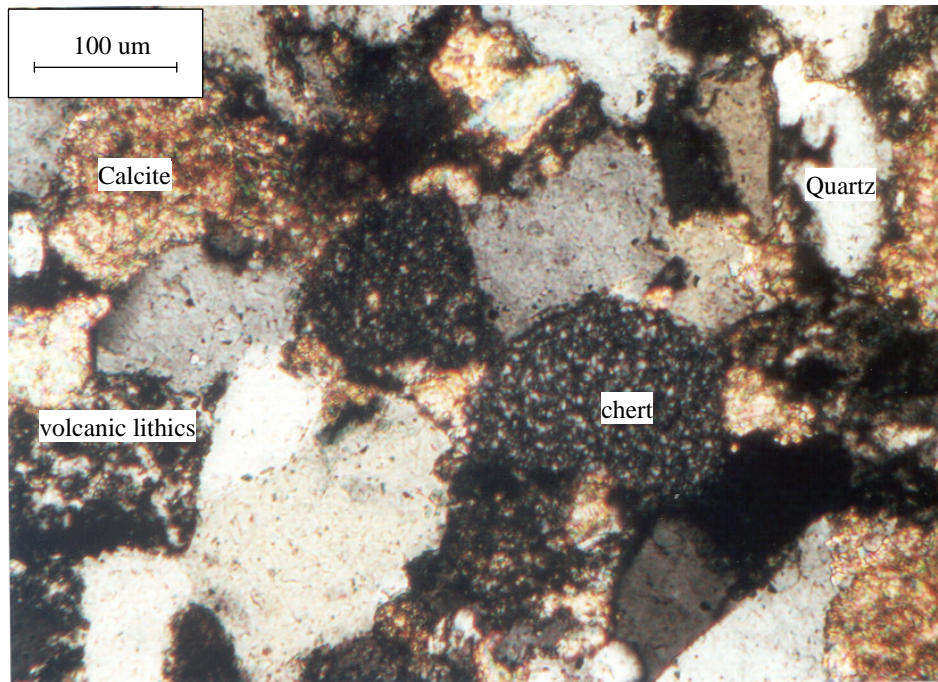


Figure 6.15 Photomicrograph (crossed polars) of volcanic and sedimentary rock fragments in the Shen87 sandstone of the Youxia Formation, Shenkeza section.

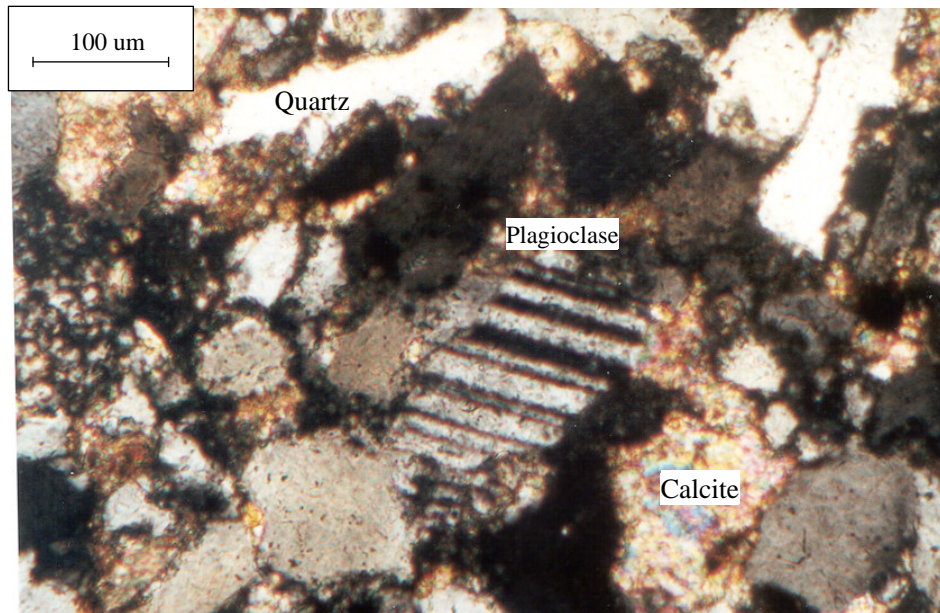


Figure 6.16 Photomicrograph (crossed polars) of a plagioclase grain in the Shen94 sandstone of the Youxia Formation, Shenkeza section.

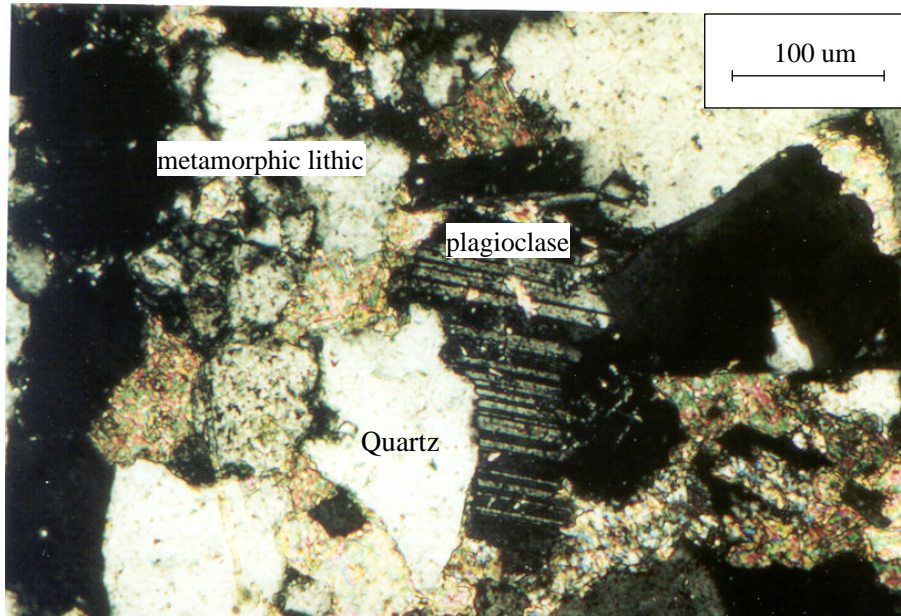


Figure 6.17 Photomicrograph (crossed polars) of a broken plagioclase and a metamorphic rock fragment in Shen88 sandstone of the Youxia Formation, Shenkeza section.

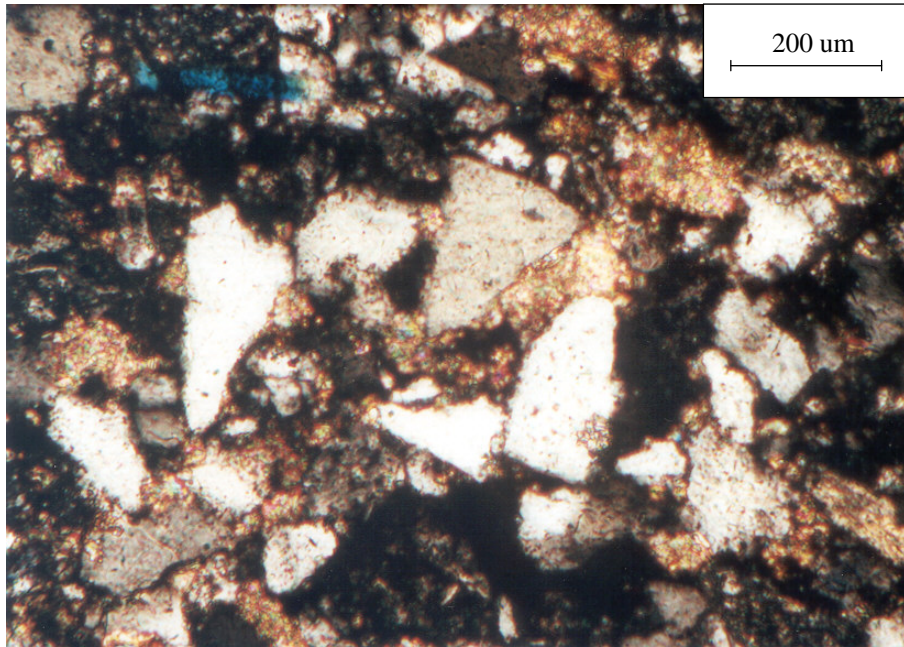


Figure 6.18 Photomicrograph (crossed polars) of angular-subangular greywackes (Shen145) of Shenkeza Formation, Shenkeza section.

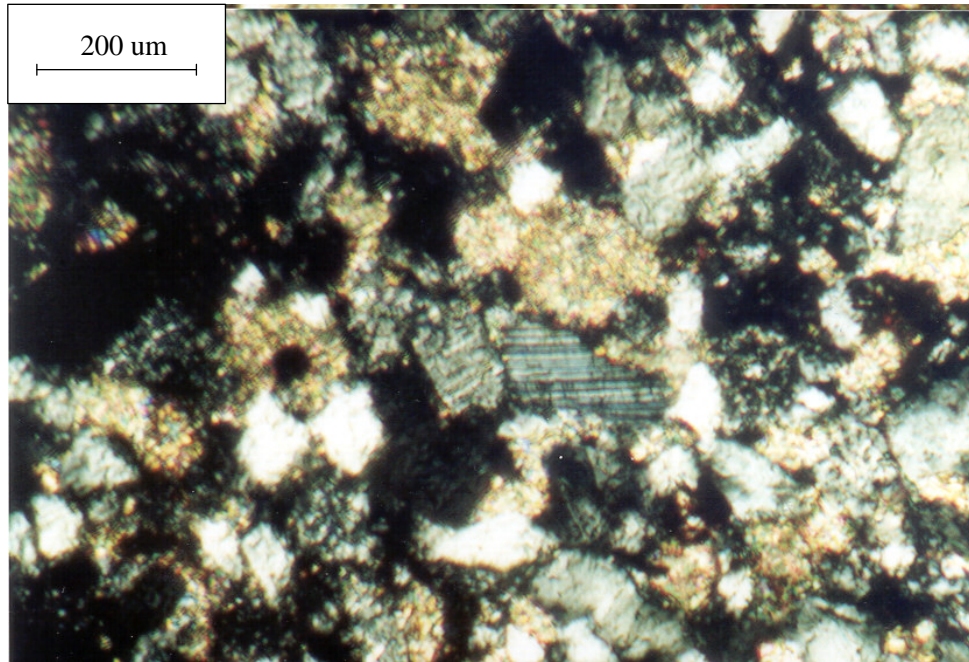


Figure 6.19 Photomicrograph (crossed polars) of angular quartz grains and a plagioclase in the Shen148 sandstone of Shenkeza Formation, Shenkeza section.

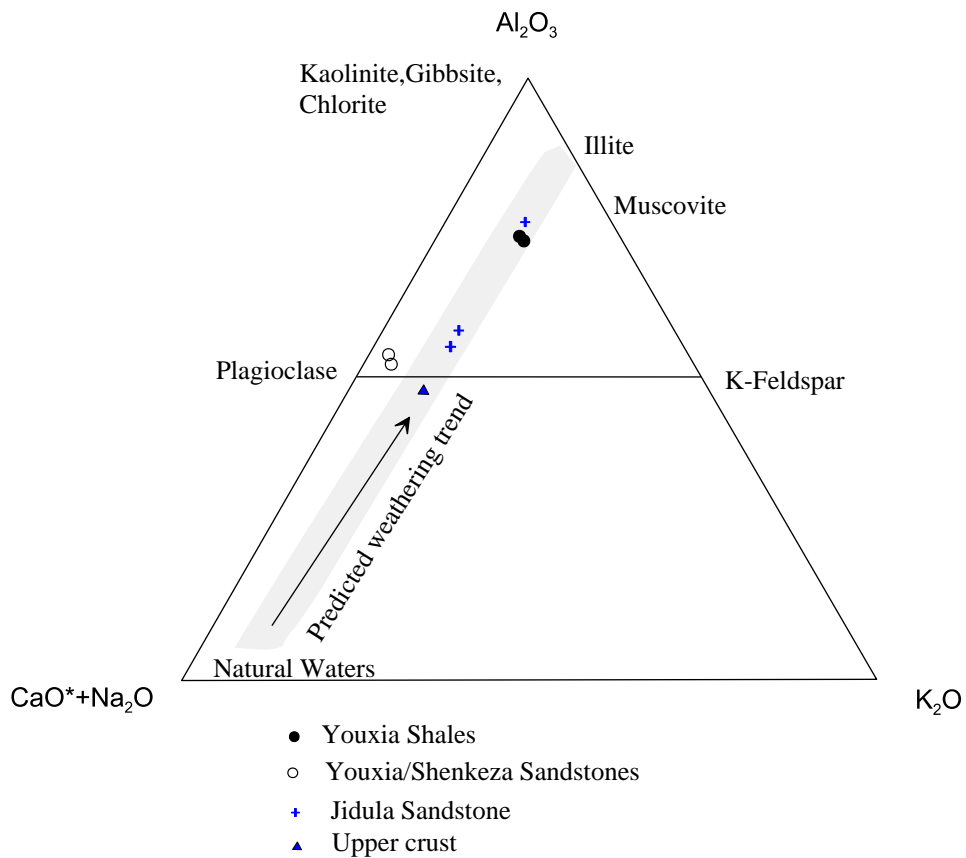


Figure 6.20 CIA ternary plot of lower Tertiary clastics in the Tingri region. Modified after Bock et al. (1998). The enrichment in Al_2O_3 and depletion of $CaO+Na_2O+K_2O$ on this plot reflects the degree of chemical weathering to which the materials have been subjected. Three analyses of the Jidula Fm. defined a linear trend encompassed in the predicted weathering trend for the average upper crustal composition while those of the Youxia Fm. do not follow the predicted weathering trend, indicating processes in addition to the weathering have affected the Youxia sediments.

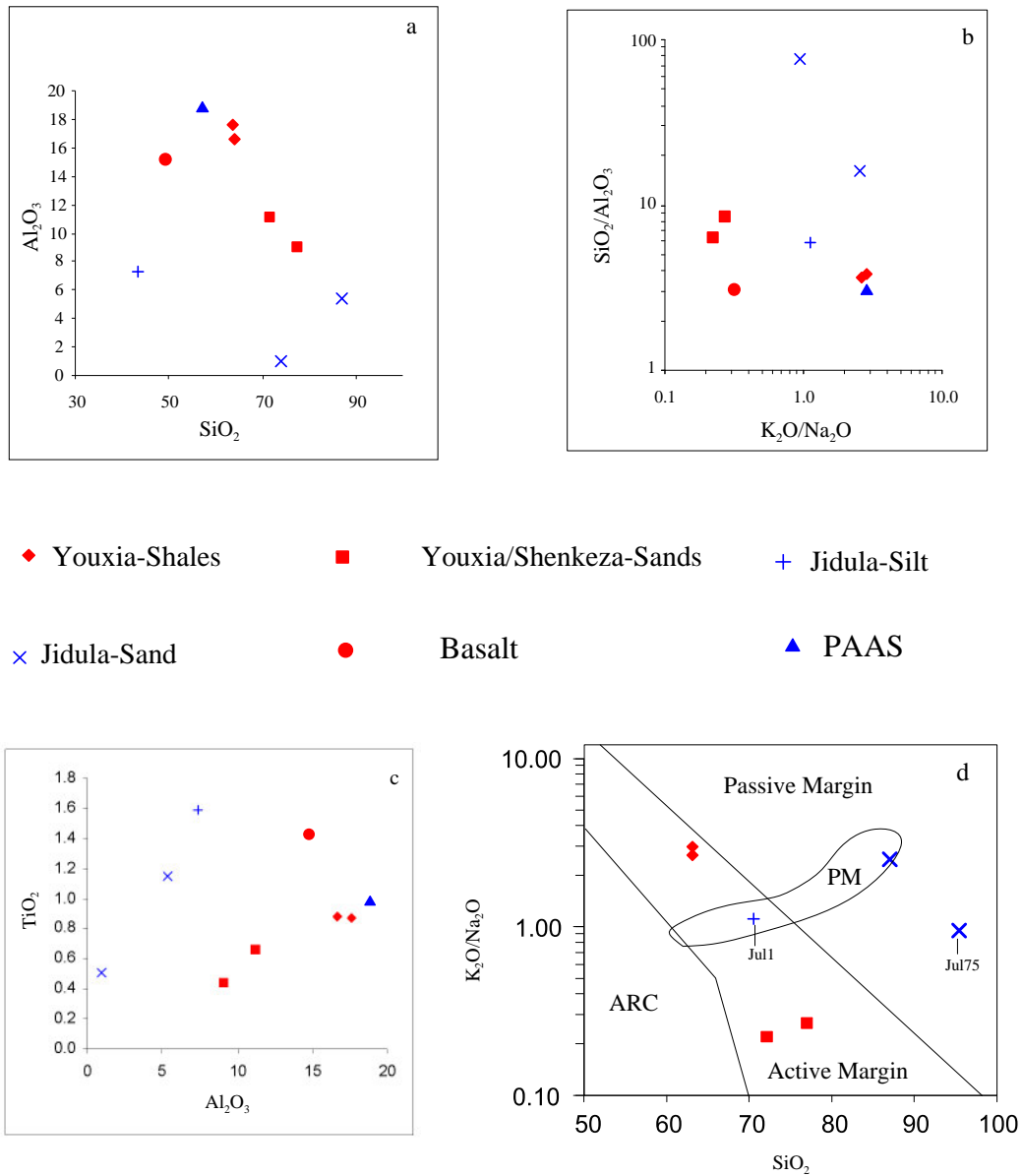


Figure 6.21 Geochemical plot of the lower Tertiary clastics in the Tingri region. a. Al_2O_3 vs. SiO_2 plot; b. SiO_2/Al_2O_3 vs. K_2O/Na_2O plot; c. Al_2O_3 vs. TiO_2 plot; d. K_2O/Na_2O vs. SiO_2 plot. Tectonic setting fields are from Roser and Korsch (1986) for Figure 6.21 d and PM is passive margin field from McLennan et al. (1990). Note in Fig 6.21d, Jul1 and Jul75 are recalculated to 100% CaO and volatile-free because of significantly high CaO contents. PAAS from Taylor and McLennan (1985), basalt from Condie (1993).

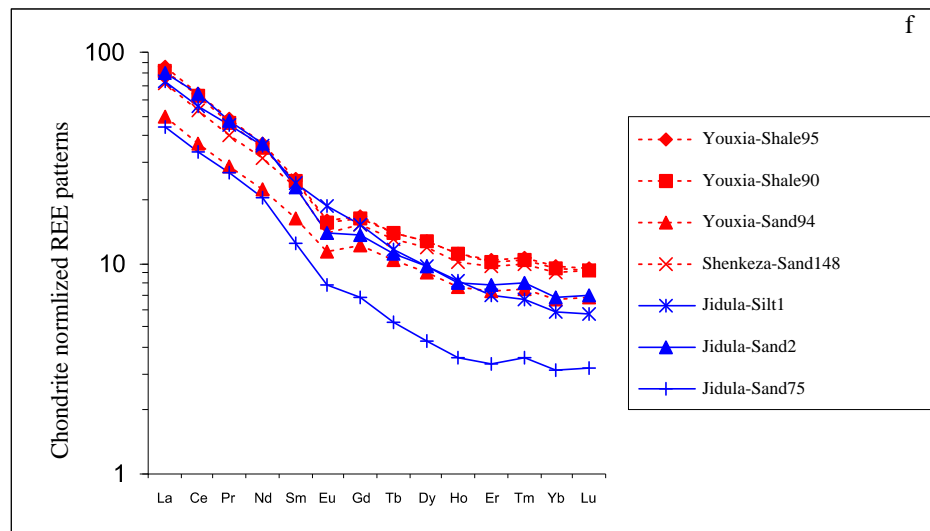
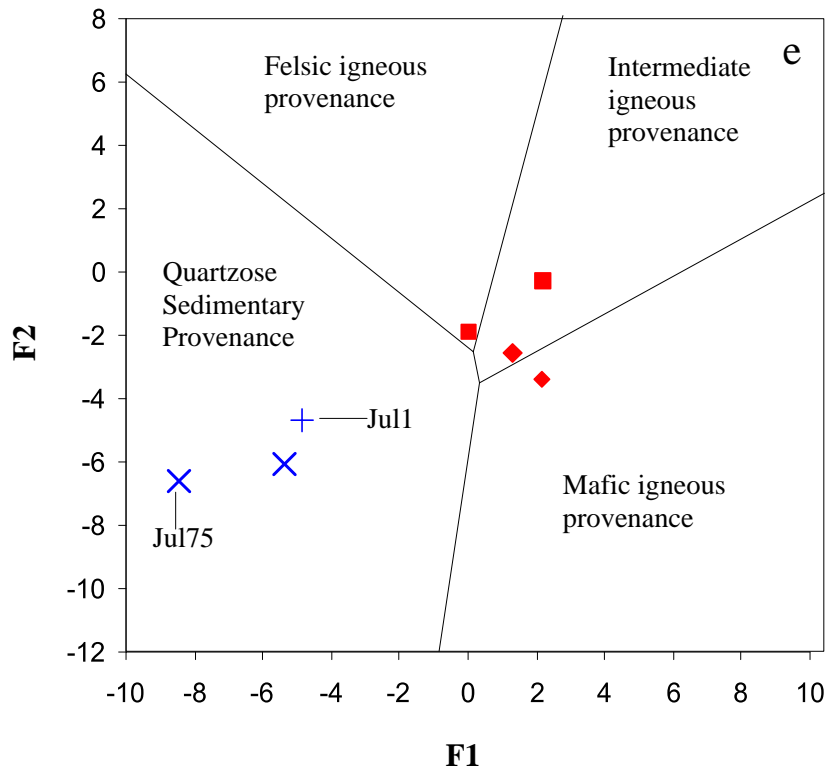
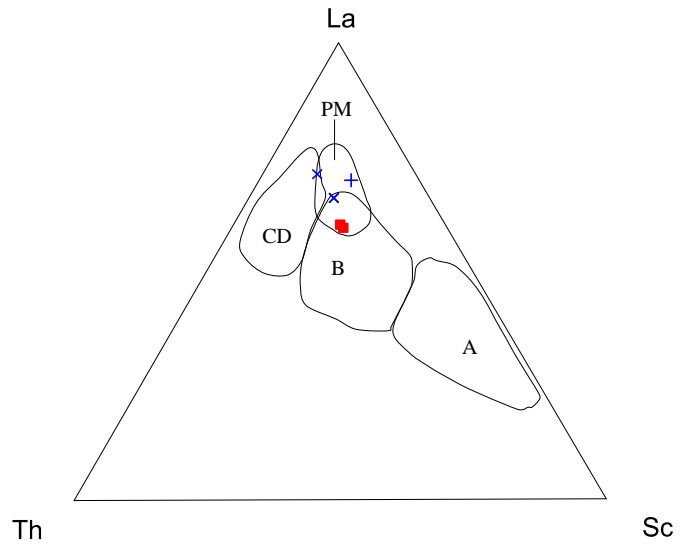
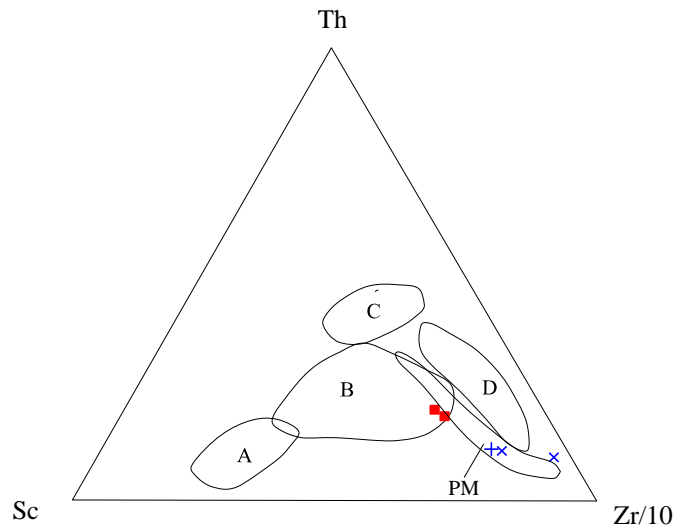


Figure 6.21(continued). Geochemical plot of the lower Tertiary clastics in the Tingri region. e. Provenance discrimination diagram; f. Chondrite-normalized REE patterns, chondritic values are those of Taylor and McLennan (1985). Tectonic setting fields are from Roser and Korsch (1988) for Figure 6.21e. Note in Figure 6.21e, Jul1 and Jul75 are recalculated to 100% CaO and volatile-free because of significantly high CaO contents.



a



b

■ Youxia/Shenkeza-Sands + Jidula-Silt × Jidula-Sand

Figure 6.22 Tectonic discrimination plots from Bhatia and Crook (1986): a. La-Th-Sc ternary plot; b. Th-Sc-Zr/10 ternary plot. Fields are A-oceanic island arc, B-continental island arc, C-active continental margin, D-passive margin. PM is the Passive margin field from McLennan et al. (1990).

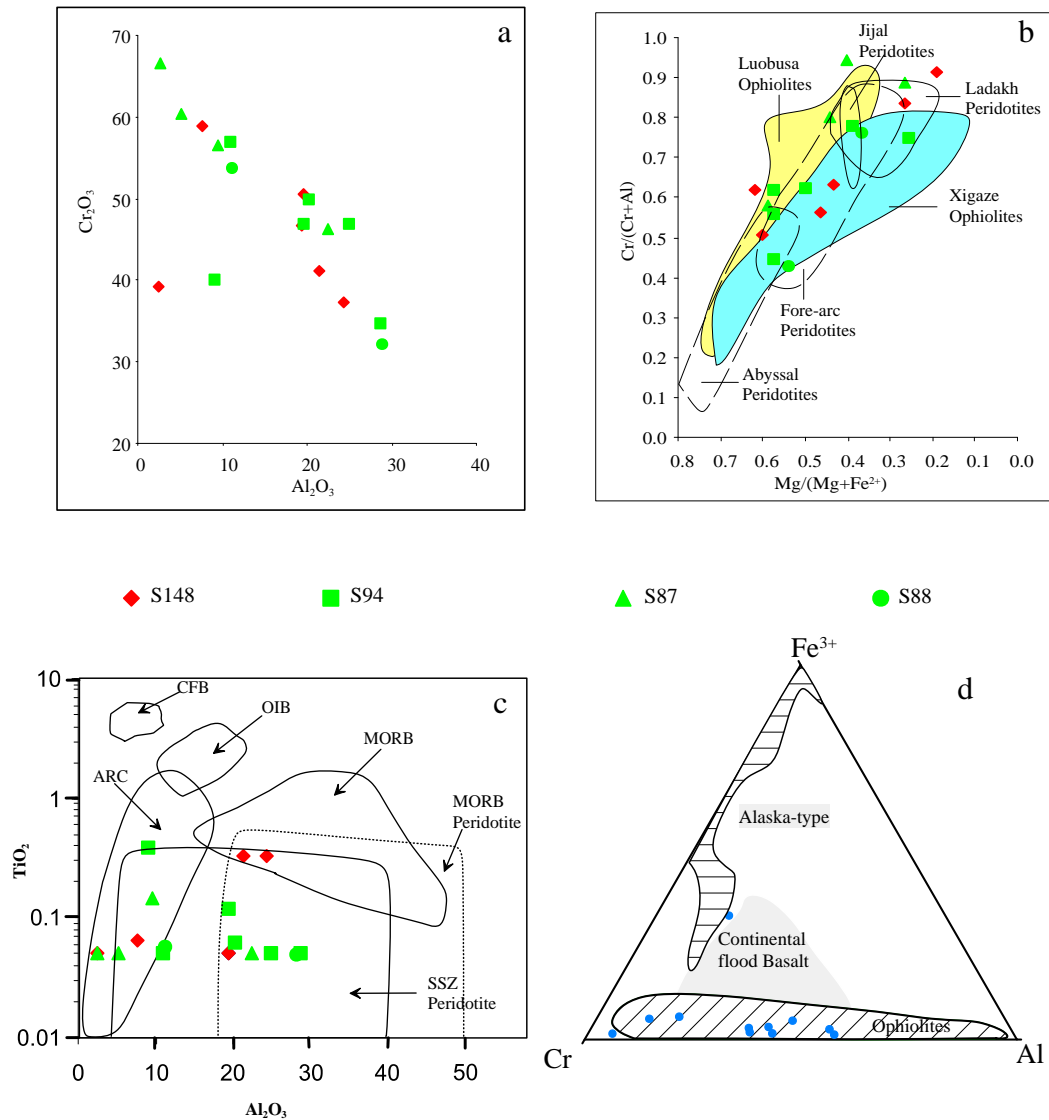


Figure 6.23 Geochemical plot of Cr-rich spinels from the Youxia and Shenkeza sandstones. a. Al_2O_3 vs. Cr_2O_3 plot, b. Cr# ($\text{Cr}/(\text{Cr}+\text{Al})$) vs. Mg# ($\text{Mg}/(\text{Mg}+\text{Fe}^{2+})$) plot, fields displayed are: Abyssal peridotites from Brindzia and Wood (1990), Fore-arc peridotites from Parkinson and Pearce (1998), Jijal Peridotites and Ladakh peridotites from Rolland et al. (2002), Luobusa ophiolites from Zhou et al. (1996), and Xigaze ophiolites from Wang et al. (2000). c. TiO_2 vs. Al_2O_3 plot, fields displayed are from Kamenetsky et al. (2001): CFB-continental flood basalt, OIB-oceanic island basalt, MORB-mid-ocean ridge basalt, ARC-volcanic island arc, SSZ-suprasubduction zone. d. Cr-Al- Fe^{3+} ternary plot, fields displayed are from Cookenboo et al.(1997).

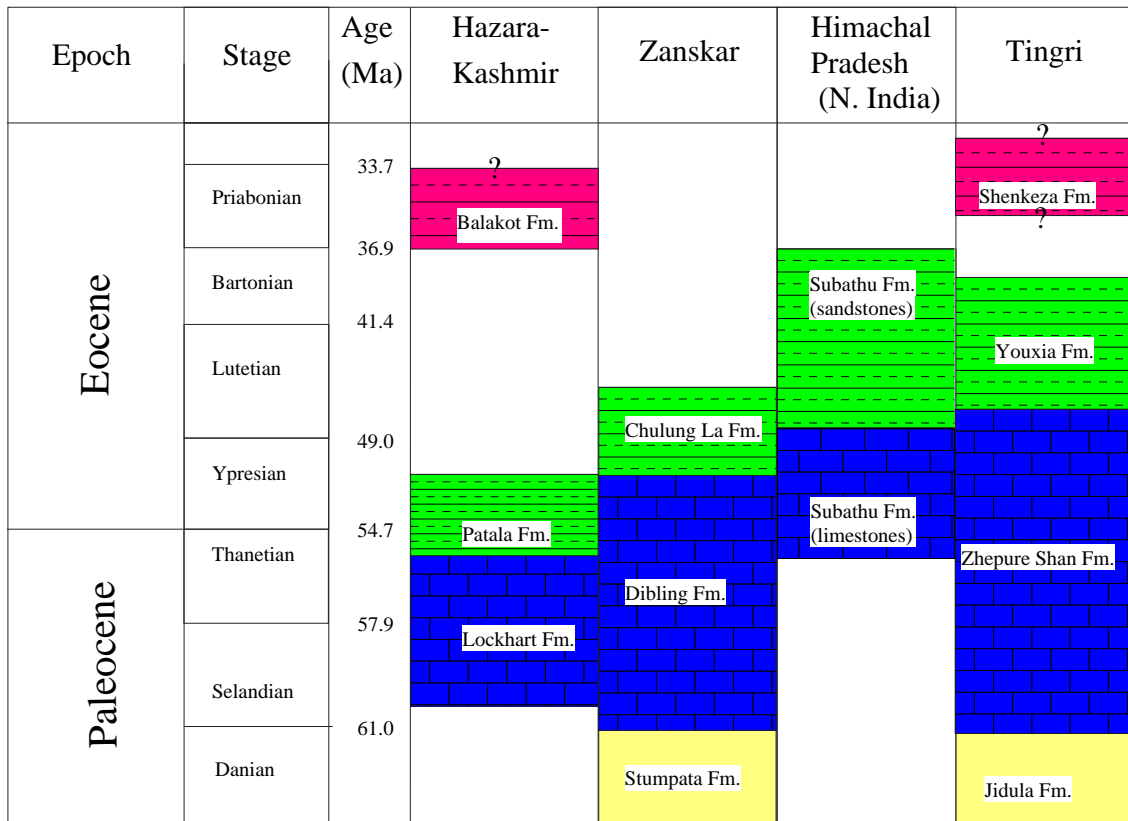


Figure 6.24 Comparison of stratigraphic columns of the Himalayan foreland basin, from Hazara-Kashmir (Bossart and Ottiger, 1989, which is modified by Najman et al. (2002)), through Zanskar (Garzanti et al., 1987, 1996), Himachal Pradesh (Najman and Garzanti, 2000), to Tingri, southern Tibet (this study). Timescale after Berggren et al. (1995).

Yellow-mature clastics of Indian passive margin; blue-carbonates of the Indian passive margin; green-marine orogenic clastics; red-non-marine redbeds.